Developmental Biology
Stem Cells and Regenerative Medicine

Negative cell cycle regulation by Calcineurin is necessary for proper beta cell regeneration in zebrafish

Reviewed Preprint

Published from the original preprint after peer review and assessment by eLife.

About eLife's process

Reviewed preprint posted
August 14, 2023 (this version)

Posted to bioRxiv
June 7, 2023

Sent for peer review
May 19, 2023

Laura Massoz, David Bergemann, Arnaud Lavergne, Célia Reynders, Caroline Désiront, Chiara Goossens, Lydie Flasse, Bernard Peers, Marianne L. Voz, Isabelle Manfroid

Zebrafish Development and Disease Models laboratory, GIGA-Stem Cells, University of Liège, Liège, Belgium • GIGA-Genomics core facility, GIGA, University of Liège, Liège, Belgium

Abstract

Stimulation of pancreatic beta cell regeneration could be a therapeutic lead to treat diabetes. Unlike humans, the zebrafish can efficiently regenerate beta cells, notably from ductal pancreatic progenitors. To gain insight into the molecular pathways involved in this process, we established the transcriptomic profile of the ductal cells after beta cell ablation in the adult zebrafish. These data highlighted the protein phosphatase calcineurin as a new potential modulator of beta cell regeneration. We showed that calcineurin overexpression abolished the regenerative response, leading to glycemia dysregulation. On the opposite, calcineurin inhibition increased ductal cell proliferation and subsequent beta cell regeneration. Interestingly, the enhanced proliferation of the progenitors was paradoxically coupled with their exhaustion. This suggests that the proliferating progenitors are next entering in differentiation. Calcineurin appears as a guardian which prevents an excessive progenitor proliferation to preserve the pool of progenitors. Altogether, our findings reveal calcineurin as a key player in the balance between proliferation and differentiation to enable a proper beta cell regeneration.

eLife assessment

This work presents some **valuable** information regarding the molecular mechanisms controlling the regeneration of pancreatic beta cells following induced cell ablation. However, the study lacks the critical lineage tracing result to support the conclusion about the origin of the regenerated beta cells. The results of the pharmacological manipulation of CaN signaling are also **incomplete**. In particular, these manipulation are not cell-specific, making it difficult to interpret and thus genetic approach is recommended.

Introduction

Blood glucose homeostasis is tightly controlled by pancreatic endocrine cells. Insulin-producing beta cells work in close association with alpha cells, which secrete glucagon, and delta cells secreting somatostatin, to maintain normal glycemia. The insulin plays a critical role in this process as it is the only hormone able to lower the glycemia. Beta cell loss is a hallmark of type 1 and of late stages of type 2 diabetes, leading to chronic hyperglycemia. Beta cell destruction is largely irreversible in human and in mammals, making the disease incurable nowadays. Nevertheless, studies in diabetic mice models uncovered promising evidences of slight recovery of beta cells via regeneration. For example, new beta cells can arise from the replication of remaining beta cells [1]. Different models of pancreas injuries revealed the plasticity of mammalian pancreatic cells. Actually, differentiated endocrine cells such as alpha cells[2] and delta cells[3] can reprogram and convert into insulin-producing cells, a process that is age dependent. Another possible source of beta cells could be de *novo* formation from pancreatic progenitors residing in the ductal compartment of the adult pancreas [4]. Lineage tracing experiments could not clearly highlight new beta cells arising from the ductal cells in the adult [4]–[6]. However, expression of the pro-endocrine marker Neurog3 was detected in the ducts in different mouse models of pancreas regeneration [4], [7], [8]. In addition, a rare population of ductal cells expressing Neurog3 has been reported to contribute to beta cell neogenesis during diabetes [9]. A recent study of single cell RNA sequencing reveal a sub-population of human ductal cells which are able to give rise to all the pancreatic cell types, including beta cells, following implantation in mice [10]. Altogether, these findings suggest that mammalian pancreatic ducts possess the intrinsic capacity to (re)generate beta cells even though this process is poorly efficient and slow, especially in adults. In contrast to mammals, zebrafish possess remarkable capacity of regeneration, independently of its age [11]–[16]. This model can therefore be exploited to identify and characterize regenerative mechanisms and ultimately induce regeneration in mammals. Based on regenerative mechanisms identified in zebrafish, several studies succeed to improve regeneration in mammals, underlying the possibility of translation from zebrafish to mammals ([17]–[21] and [22], for review).

In zebrafish, the nitroreductase (NTR)/nitroaromatic prodrug system is widely used. In this technique, the combination of cell type-specific NTR expression and nitroaromatic prodrug exposure allow for controlled and targeted cell ablation [23], [24]. When NTR is expressed under the control of the *insulin* (*ins*) promoter (*Tg*(*ins:NTR-mCherry*) [25]), beta cell destruction is complete within 3 days following the treatment in adult fish, which correlate with a peak of hyperglycemia [26], [27]. The regeneration of beta cells upon ablation is spontaneous and fast and the glycemia is normalized within two weeks [13], [29]. Similar to mice, new beta cells can arise through proliferation of surviving beta cells [28] as well as through the contribution of alpha cells [29], [30] and delta cells[31], [32], underscoring the overall conservation of these processes from zebrafish to mammals. Nevertheless, unlike mammals, the presence of pancreatic progenitors in the ducts is well established in both larval [33] and adult zebrafish [26], [27]. Lineage tracing experiments pointed out that ductal cells and centroacinar cells (CACs) give rise to new beta cells [26], [33]. In adults, duct-derived beta cells start to be detected between 7 and 10 days following beta cell ablation [26], [27].

Notch signaling is a key player regulating the differentiation of duct-associated progenitors into endocrine cells. Larval duct cells as well as adult CACs display strong Notch activity [26], [34]. This signaling pathway has a central role in beta cell genesis during both development [35] and regeneration [33] by repressing endocrine differentiation. In zebrafish, different levels of Notch activity determine the behavior of the pancreatic progenitors. While a high level of Notch activity maintains cells in quiescence, a moderate level induces the entry in the cell cycle and proliferation whereas a low level drives endocrine differentiation of the progenitor cells [35]. A steep decrease of Notch activity pushes the progenitors to differentiate prematurely, bypassing the amplification step and leading to their depletion [35]. Repression of the Notch signaling by

mTor, activated by glucose and nutrients, hence promotes beta cell formation and regeneration from ductal progenitors [33]. While Notch and mTor signaling are crucial for this process, there is still a need to establish a global view of the molecular mechanisms regulating beta cell regeneration.

To identify early events regulating ductal-derived beta cell regeneration, we determined the transcriptomic signature of ductal cells from adult zebrafish following beta cell destruction. Our data highlighted an upregulation of the Calcineurin (CaN) pathway. To elucidate CaN function in beta cell regeneration, we both repressed and activated CaN pathway. We showed that CaN regulates beta cell neogenesis in the ducts during regeneration, by modulating progenitor proliferation. Together, our findings underline that CaN fine tunes the balance between progenitor proliferation and beta cell differentiation to guarantee proper regeneration.

Results

Transcriptomic profiling of ductal cells after beta cell destruction highlights regulation of calcineurin pathway

To gain a better understanding of the molecular mechanisms underlying the regeneration of beta cells from the ducts, we determined the transcriptional landscape of ductal cells by RNA-sequencing after beta cell ablation in adults. To selectively ablate the beta cells, we used the *Tg*(*ins:NTR-mCherry*) transgenic fish and the ductal cells were labelled through the *Tg*(*nkx6.1:GFP*) reporter line [27] in which GFP marks the ductal tree and associated multipotent pancreatic progenitors [27]. More precisely, 3 to 4 fishes were treated with the pro-drug MTZ at 10mM overnight, to induce ablation of beta cells or with DMSO for the non-ablated controls. Ablation was confirmed by blood glucose measurement before collection of the pancreas. To capture the early events triggered by the destruction of beta cells, we generated the transcriptome of the ducts 3 days post ablation treatment (dpt), *i.e.* before beta cell neogenesis. Differential gene expression analysis revealed that 1866 genes are up-regulated and 1515 genes down-regulated in the ductal cell of fish treated with MTZ compared to control (pAdj < 0.05). According to Gene Ontology analysis, the most enriched pathways among the up-regulated genes were DNA replication and cell cycle (**Figure 1A**). This further corroborates our previous findings and those of others regarding the activation of duct-associated progenitors' proliferation in response to beta cell ablation[26], [27]. As expected, the Notch pathway was enriched in the down-regulated genes [33], [35] (**Figure 1B**). Intriguing in a context of strong proliferative response, we found an enrichment of the cellular senescence signature (**Figure 1A**). We looked further in the genes associated with this signature. Among them were found several components of the calcineurin signaling pathway such as *nfatc3b*, *ppp3ccb* (the catalytic subunit of Calcineurin*), itpr2* and *calm3b* **(Figure 1C)**. In addition to these genes related to cellular senescence, our RNAseq studies revealed the modulation of other genes from the CaN canonical pathway (**Figure 1D, genes in green**), underlying its potential role in beta cell regeneration. Calcineurin (CaN) is a highly conserved calcium/calmodulin dependent Ser/Thr phosphatase, involved in numerous biological process including fin regeneration and beta cell function, [36]–[39]. This prompted us to investigate the role of CaN in beta cell regeneration Previous RNAseq data performed in our laboratory indicate that CaN (*ppp3cca/b*) and NFATc3 (*nfatc3a/b*) are mainly express in endocrine cells [40] (**Figure 1A supplemental**), which is in accordance with the role of CaN/NFAT signaling in beta cells [41]. CaN genes (*ppp3cca/b*) as well as *nfatc3b,* are express at lower levels in the ducts at basal state but their expression is induced in response to beta cell destruction (**Figure 1B supplemental**).

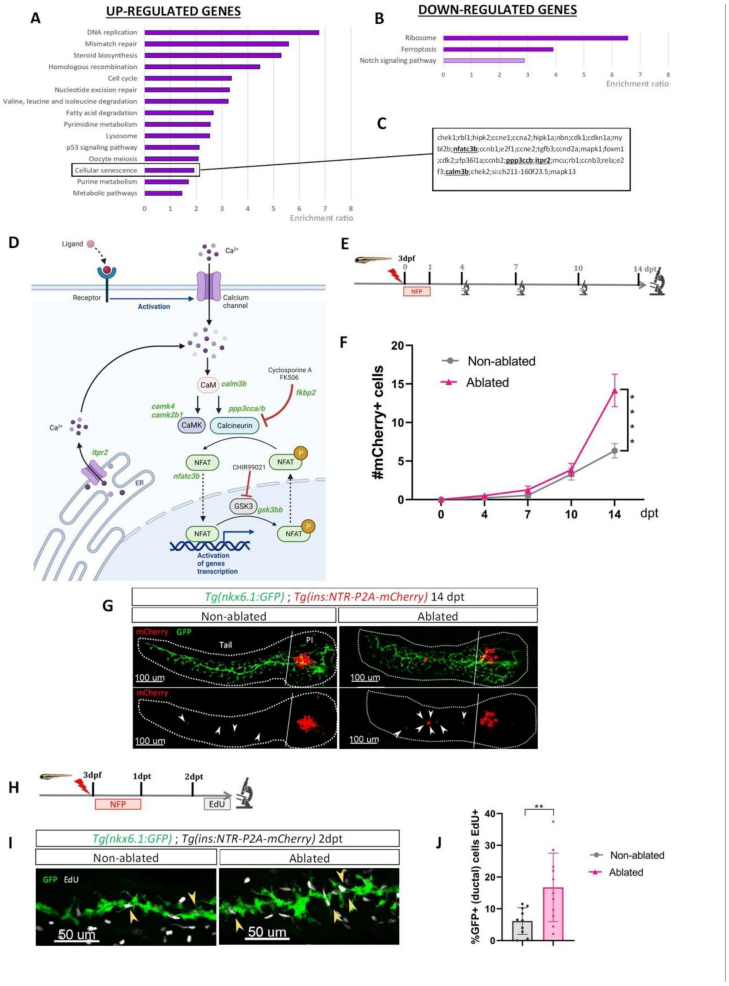

Figure 1

Transcriptomic profiling of ductal cells during beta cell regeneration and validation in larvae

A-B) Enrichment ratio of selected non-redundant signatures of KEGG pathways overrepresented in ductal cells after beta cells ablation (UP – A and DOWN-B) compared to ductal cells without beta cells ablation. Gene Ontology (GO) terms were identified using ORA analysis by WebGestalt (Liao et al., 2019) using the list of DE genes provided by DESeq. The light color for Notch pathway means p-value = 0.11.

C) List of genes associated with the signature of cellular senescence from A-B. Genes related to CaN pathway are in bold.

D) Calcineurin canonical pathway with genes in green that are modulated in transcriptomic data from A-B.

E) Experimental design for regeneration test in larvae. Briefly, after nifurpirinol treatment from 3 to 4dpf, larvae were fixed and analyzed at 4-7-10 and 14 days post treatment (dpt).

F) Graph representing the mean number of mCherry+ beta cells in the pancreatic tail of *Tg(ins:NTR-P2A-mCherry) ; Tg(nkx6.1:GFP)* at 0-4-7-10 and 14 dpt. The gray spheres represent non-ablated conditions and the pink triangles the ablated condition. Data are presented as mean values ± SEM. One-way ANOVA test with Tukey's multiple comparison test, ****p-value>0.0005.

G) Whole mount fluorescent immunohistochemistry (GFP and mCherry) of the pancreas of *Tg(ins:NTR-P2A-mCherry) ; Tg(nkx6.1:GFP)* larvae at 14dpt. 3D projection (stack) of one non-ablated and one ablated representative samples. The principal islet (PI) and the pancreatic tail are shown. Arrows point out mCherry+ beta cells in the pancreatic tail. Scale 100µM.

H) Experimental design for EdU assay in larvae. After NFP treatment for 3 to 4dpf, larvae were exposed to EdU at 2dpt before fixation for analysis.

I) Whole mount fluorescent immunohistochemistry (GFP and EdU) of the pancreatic tail of *Tg(ins:NTR-P2A-mCherry) ; Tg(nkx6.1:GFP)* larvae at 2dpt. 3D projection (stack) of one non-ablated and one ablated representative samples. Arrows point out GFP+ duct cells EdU+ in the pancreatic tail. Scale 50µM.

J) Barplot representing the percentage of GFP+ ductal cells which incorporated EdU+ in non-ablated and ablated conditions. Data are presented as mean values ± SD. T-test. **p-value>0.005.

Calcineurin activity regulates the ductal regenerative response

To evaluate the role of CaN in beta cell regeneration, more specifically derived from ductal progenitors, we have chosen to use young larvae, where regenerated beta cells in the pancreatic tail arise exclusively from the ducts [33]. In response to beta cells ablation, the intrapancreatic ducts undergo a ductal regenerative response whereby differentiation toward the endocrine fate is increased [33]. We first determined the rate of beta cell neogenesis from the ducts in response to a single acute ablation of beta cells as we performed in adults. We treated *Tg*(*ins:NTR-P2A-mCherry*); *Tg*(*nkx6.1:GFP*) larvae with nifurpirinol (NFP) from 3 to 4 dpf mCherry+ beta cells were quantified in the GFP+ ducts present in the tail at several time points: 4, 7, 10 and 14 dpt (**Figure 1E**). Duct-associated beta cells started to be detected in non-ablated larvae between 7 and 10 dpt (**Figure 1F**) and the number of beta cells slowly increased until 14 dpt (**Figure 1F, 1G**). In ablated larvae, the increase became more pronounced from 10 dpt onwards (**Figure 1F, 1G**), indicating faster endocrine differentiation. This experiment establishes that the ductal regenerative response is detectable between 10 and 14 days after the ablation of beta cells, performed at 3 dpf. We next wanted to determine if ductal cell proliferation is activated in response to beta cell destruction in larvae as in adult fish. We exposed *Tg(ins:NTR-P2A-mCherry); Tg(nkx6.1:GFP)* larvae to EdU the second day following ablation (**Figure 1H**). In ablated larvae, the proportion of GFP+ ductal cells EdU+ (in S-phase) was higher compared to non-ablated larvae (**Figure 1I, 1J**). This result shows that acute beta cell ablation in larvae rapidly activates ductal cell proliferation, as previously reported in adult zebrafish.

As our transcriptomic data from adult zebrafish revealed modulation of CaN pathway at 3 dpt, we treated *Tg*(*ins:NTR-P2A-mCherry*); *Tg*(*nkx6.1:GFP*) larvae from 1 to 3 dpt after beta cell ablation, with a CaN inhibitor, the Cyclosporin A (CsA) [39] (**Figure 2A**). The number of newly formed beta cells was monitored in the tail from 4 to 14 dpt. CsA enhanced beta cell formation at 10 dpt (**Figure 2B-D**). However, this effect appears to be transient since no discernible difference was observed between the control and CsA-treated larvae in regeneration at the latest time point, suggesting an acceleration of the regenerative response (**Figure 2B**, **Figure 2A supplemental**). Interestingly, CsA did not affect beta cell differentiation in non-ablated larvae indicating that CsA only acts in a regenerative context (**Figure 2B-D**). Of note, CsA increased as well the number of regenerated beta cells in the principal islet (**Figure 2B supplemental**).

We next tested the effect of CsA on endocrine progenitors in a regenerative context. We induced regeneration in Tg(*neurod1:GFP*) larvae where the GFP is expressed in both endocrine progenitors and mature endocrine cells. We first assessed generation of GFP cells at different time points (**Figure 2D supplemental**) and showed that CsA induced an increase of neurod1+ cells from 4 dpt. The increase was still detectable at least until 10dpt **(Figure 2E**, **Figure 2E supplemental)**. To determine if these additional cells result from their own proliferation, we performed a pulse of EdU just before analysis (**Figure 2D supplemental**). We observed that CsA did not affect the neurod1+ proliferation rate that is very low at these stages (**Figure 2F**). As a consequence, the effect of CsA cannot be explained by endocrine cell proliferation but rather by neogenesis from progenitors. As CsA affects pro-endocrine cells formation, we next wondered if the increased cell formation induced by CsA is specific to beta cells. Treatment with CsA was performed as previously and delta and alpha cells were detected by immunofluorescence. Interestingly, CsA did not affect alpha nor delta1.1 cells neogenesis in response to beta cell ablation (**>Figure 2F-G supplemental**). Overall, these experiments showed that CsA affects specifically the beta cells and their endocrine progenitors.

CaN over-activation abolishes the regenerative response

We then wondered if an opposite regulation of CaN *i.e.* its activation impacts as well the regenerative response. To that end, we generated a transgenic line Tg(*hsp70:GFP-P2A-ppp3ccCA*) that allows ubiquitous expression of a constitutively active form of CaN^{CA} ($ppp3cc^{CA}$) upon heat shocks. Beta cell ablation was triggered in Tg($hsp70$:GFP-P2A-$ppp3cc^{CA}$); Tg(*ins:NTR-P2A-mCherry*);

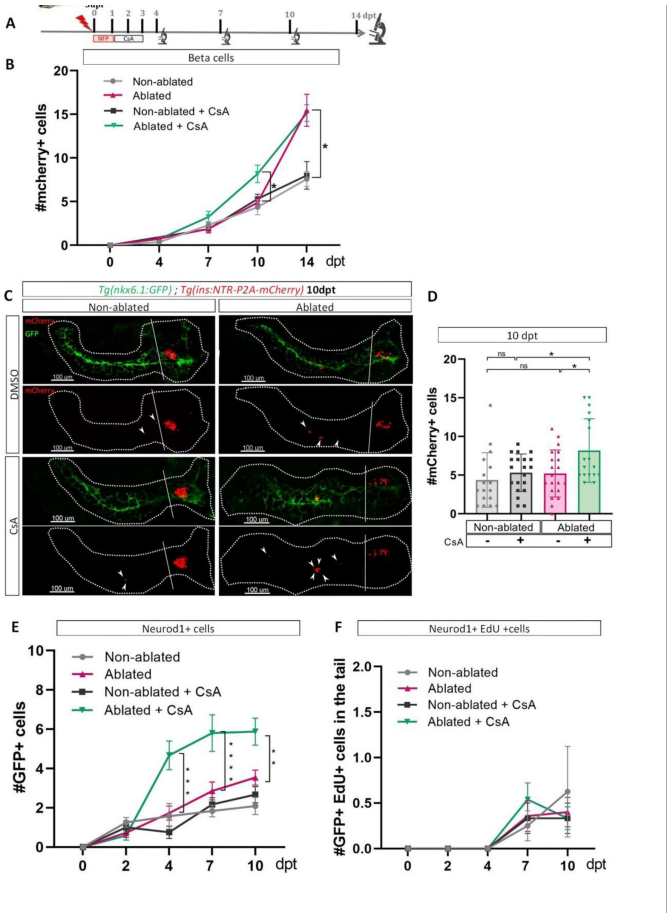

Figure 2

Calcineurin inhibition with CsA increases the ductal regenerative response

A) Experimental design for regeneration test in larvae with CsA treatment. Briefly, after nifurpirinol treatment from 3 to 4dpf, larvae were treated with CsA from 1 to 3dpt and fixed and analyzed at 4-7-10 and 14 days post treatment (dpt).
B) Graph representing the mean number of mCherry+ beta cells in the pancreatic tail of *Tg(ins:NTR-P2A-mCherry) ; Tg(nkx6.1:GFP)* at 0-4-7-10 and 14 dpt. The gray spheres represent non-ablated condition ; the pink triangles represent the ablated condition ; the black squares CsA condition and inverted green triangles ablated + CsA condition. Data are presented as mean values ± SEM. Two-way ANOVA test with Sidak's multiple comparisons test, *p-value>0.05.
C) Whole mount fluorescent immunohistochemistry (GFP and mCherry) of the pancreas of *Tg(ins:NTR-P2A-mCherry) ; Tg(nkx6.1:GFP)* larvae at 10dpt. 3D projection (stack) of non-ablated and ablated larvae treated with DMSO or CsA representative samples. The principal islet (PI) and the pancreatic tail are shown. Arrows point out mCherry+ beta cells in the pancreatic tail. Scale 100µM.
D) Barplot representing the number of number of mCherry+ beta cells in the pancreatic tail of *Tg(ins:NTR-P2A-mCherry) ; Tg(nkx6.1:GFP)* larvae at 10dpt. The gray spheres represent non-ablated condition ; the pink triangles represent the ablated condition ; the black squares CsA condition and inverted green triangles ablated + CsA condition. Data are presented as mean values ± SD. Two-way ANOVA with Tukey's multiple comparison test, *p-value>0.05.
E) Graph representing the mean number of GFP+ neurod1+ cells in the pancreatic tail of *Tg(ins:NTR-P2A-mCherry) ; Tg(neurod1:GFP)* at 0-4-7 and 10 dpt. The gray spheres represent non-ablated condition ; the pink triangles represent the ablated condition ; the black squares CsA condition and inverted green triangles ablated + CsA condition. Data are presented as mean values ± SEM. Two-way ANOVA test with Sidak's multiple comparisons test, **p-value>0.005; *** p-value>0.0005; **** p-value>0.00005.
F) Graph representing the mean number of GFP+ neurod1 EdU+ cells in the pancreatic tail of *Tg(ins:NTR-P2A-mCherry) ; Tg(neurod1:GFP)* at 0-4-7 and 10 dpt. The gray spheres represent non-ablated condition ; the pink triangles represent the ablated condition ; the black squares CsA condition and inverted green triangles ablated + CsA condition. Data are presented as mean values ± SEM.

Tg(*ins:NTR-P2A-mCherry*); Tg(*nkx6.1:GFP*) larvae from 3 to 4 dpf and CaN^{CA} expression was induced by four successive heat-shocks from 1 to 3 dpt (**Figure 3A**). The overexpression of CaN^{CA} after ablation impaired the regenerative response at 14 dpt (**Figure 3B-C**). Similar results were obtained with Tg(*UAS:GFP-P2A-ppp3cc*^{CA}); Tg(*cftr:gal4*)[45] ; Tg(*ins:NTR-P2A-mCherry*) larvae in which CaN^{CA} is constitutively and specifically overexpressed in the ducts within the pancreas (**Figure 3D-E**). Importantly, the structure of the ducts was similar in CaN^{CA} overexpressing larvae compared to Tg(*nkx6.1:GFP*) controls (**Figure 3D**), suggesting that the suppression of the regenerative response in CaN^{CA}-overexpressing larvae was not due to morphogenetic defects during ductal growth. This result strongly suggest that CaN acts directly in the ducts to regulate beta cell regeneration while it is not necessary for normal beta cell differentiation.

CaN regulates beta cell differentiation induced by Notch inhibition in absence of regeneration

Our transcriptomic data showed that the Notch pathway is downregulated in ductal cells during beta cell regeneration (**Figure 1**). As the level of Notch activity determines the behavior of ductal cells [33] from quiescence to proliferation and subsequently to beta cell differentiation, we tested whether calcineurin acts together with the Notch pathway on a common pool of ductal progenitors. To inhibit the Notch pathway, we treated larvae with several concentrations of the gamma-secretase inhibitor LY411575 from 3 to 4dpf in absence of regeneration. The activity of CaN was inhibited by CsA during the same timeframe (**Figure 4A**). As previously, we used reporter lines for beta and ductal cells *Tg*(*ins:NTR-P2A-mCherry*); *Tg*(*nkx6.1:GFP*) and the number of secondary beta cells was analyzed at 6dpf (**Figure 4A**). As expected, the number of beta cells progressively rose as the concentration of the Notch inhibitor increased (**Figure 4B**). Combined treatment with CsA fostered the differentiation of beta cells between 1 and 10 µM LY411575 but did not result in further increase at 15 µM LY411575 (**Figure 4B**), suggesting that CaN is important within a permissive window of Notch activity. Since we overserved the highest synergistic effect at 5µM of LY411575, we used this concentration for the following experiments (**Figure 4C-D**). It is worth noting that combined treatment of LY411575 (5uM) and another CaN inhibitor, FK506, resulted in the same synergistic increase of beta cell differentiation (**Figure 4A-B supplemental**), confirming that the effect is due to CaN inhibition. The combined effect of Notch and CaN inhibition is transient as it is not observed at 7dpf anymore (**Figure 4E**). Therefore, as observed in regenerative conditions (**Figure 2B**), CaN inhibition accelerates beta cell neogenesis induced by Notch repression.

To determine to which extent CaN pathway can modulate Notch induced beta cell neogenesis, we activated CaN^{CA} overexpression in *Tg*(*hsp70:GFP-P2A-ppp3cc*^{CA}*); Tg*(*ins:NTR-P2A-mCherry*) larvae by an heat-shock at 3 dpf and treated them with LY411575 (**Figure 4C supplemental**). CaN^{CA} overexpression resulted in a lowered beta cell formation induced by Notch inhibition (**Figure 4D supplemental**), revealing that CaN activation counterbalanced the effects of Notch inhibition. Using our previous settings of Notch and CaN inhibition, we next wondered if the canonical pathway downstream of CaN was involved in the enhancement of beta cell differentiation. To activate NFAT, a well-known target of CaN, we used CHIR99021 allowing a stabilization of the active form of NFAT (**Figure 1D**). We found that CHIR99021 rescued the effect of CsA (**Figure 4D supplemental**), suggesting that CaN inhibition increases beta cell neogenesis at least partially by the regulation of NFAT. Overall, these results reveal that CaN regulates beta cell formation in pro-endocrinogenic context, such as induced by a low level of Notch activity. Moreover, it suggests that both CaN and Notch pathway act on a common pool of ductal progenitors to regulate beta cell neogenesis.

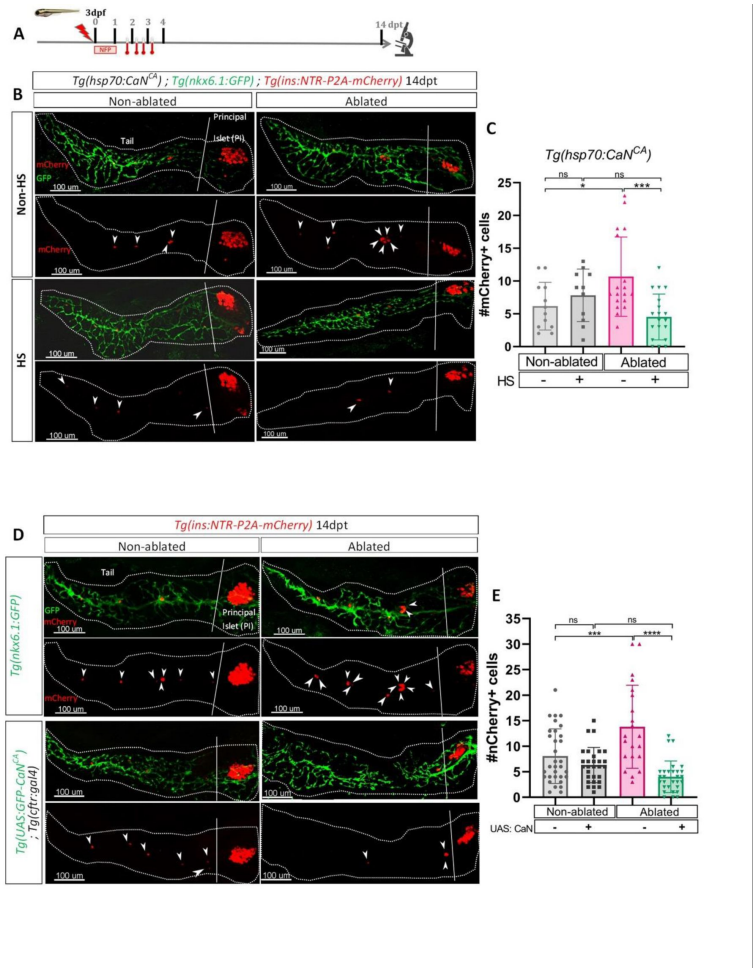

Figure 3

Transgenic mediated overexpression of calcineurin abolish the ductal regenerative response

A) Experimental design for regeneration test in larvae with heat-shocks. Briefly, after nifurpirinol treatment from 3 to 4dpf, four heat shock were performed from 1 to 3dpt and larvae were fixed and analyzed at 14dpt.
B) Whole mount fluorescent immunohistochemistry (GFP and mCherry) of the pancreas of *Tg(hsp70:CaN^{CA})*; *Tg(ins:NTR-P2A-mCherry); Tg(nkx6.1:GFP)* larvae at 14dpt. 3D projection (stack) of one non-ablated and one ablated with or without heat-shock representative samples. The principal islet (PI) and the pancreatic tail are showed. Arrows point out mCherry+ beta cells in the pancreatic tail. Scale 100µM.
C) Barplot representing the mean number of mCherry+ beta cells in the pancreatic tail of *Tg(hsp70:CaN^{CA})*; *Tg(ins:NTR-P2A-mCherry); Tg(nkx6.1:GFP)* larvae at 14dpt. The gray spheres represent non-ablated condition ; the pink triangles represent the ablated condition ; the black squares heat-shock condition and inverted green triangles ablated + heat-shock condition. Data are presented as mean values ± SD. Two-way ANOVA with Tukey's multiple comparisons test, *p-value>0.05, *** p-value>0.0005, ns = non-significant.
D) Whole mount fluorescent immunohistochemistry (GFP and mCherry) of the pancreas of larvae at 14dpt. 3D projection (stack) of *Tg(ins:NTR-P2A-mCherry) ; Tg(nkx6.1:GFP)* one non-ablated and one ablated representative control samples and *Tg(UAS:CaN^{CA})*; *Tg(ins:NTR-P2A-mCherry) ; Tg(cftr:gal4)* one non-ablated and one ablated representative samples. The principal islet (PI) and the pancreatic tail are showed. Arrows point out mCherry+ beta cells in the pancreatic tail. Scale 100µM.
E) Barplot representing the mean number of mCherry+ beta cells in the pancreatic tail of larvae at 14dpt. The gray spheres represent non-ablated *Tg(ins:NTR-P2A-mCherry) ; Tg(nkx6.1:GFP)* condition ; the pink triangles represent the ablated *Tg(ins:NTR-P2A-mCherry) ; Tg(nkx6.1:GFP)* condition ; the black squares non-ablated *Tg(UAS:CaN^{CA})*; *Tg(ins:NTR-P2A-mCherry) ; Tg(cftr:gal4)* condition and inverted green triangles ablated *Tg(UAS:CaN^{CA})*; *Tg(ins:NTR-P2A-mCherry) ; Tg(cftr:gal4)* condition. Data are presented as mean values ± SD. Two-way ANOVA with Tukey's multiple comparison test, *** means p-value>0.0005, **** p-value>0.00005, ns = non-significant.

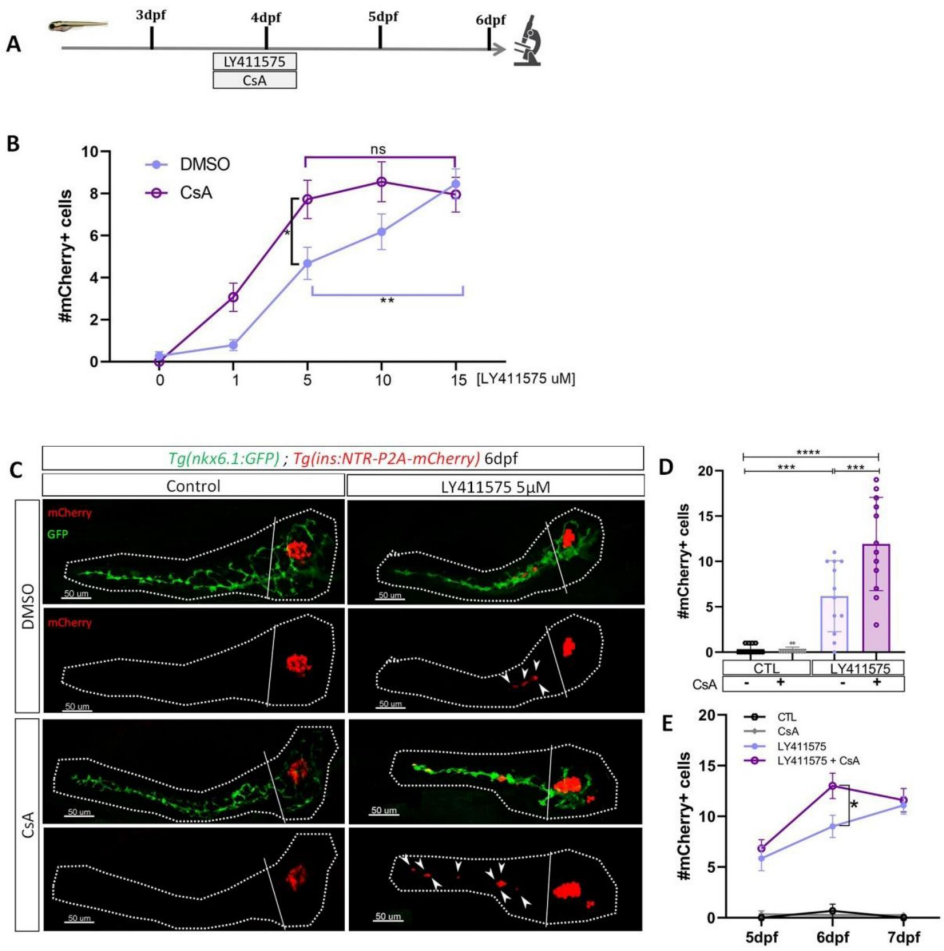

Figure 4

CaN repression potentializes the effect of Notch inhibition on beta cell formation

A) Experimental design for Notch inhibition test in non-ablated condition. Larvae were treated concomitantly with LY411575 (Notch inhibitor) and CsA from 3 to 4dpf and were fixed and analyzed at 6dpf.
B) Graph representing the mean number of mCherry+ beta cells in the pancreatic tail of *Tg(ins:NTR-P2A-mCherry) ; Tg(nkx6.1:GFP)* larvae at 6 dpf depending the concentration of LY411575. The blue dots represent LY411575; and purple combination of LY411575 and CsA. Data are presented as mean values ± SEM. Two-way ANOVA test with Sidak's multiple comparison test, *p-value>0.05, **p-value>0.05, ns = non-significant.
C) Whole mount fluorescent immunohistochemistry (GFP and mCherry) of the pancreas of *Tg(ins:NTR-P2A-mCherry) ; Tg(nkx6.1:GFP)* larvae at 6dpf. 3D projection (stack) of one control (without any treatment) ; one CsA-treated ; one LY411757-treated and one with both CsA and LY411575 treated larvae. The principal islet (PI) and the pancreatic tail are showed. Arrows point out mCherry+ beta cells in the pancreatic tail. Scale 50µM.
D) Barplot representing the mean number of mCherry+ beta cells in the pancreatic tail of *Tg(ins:NTR-P2A-mCherry) ; Tg(nkx6.1:GFP)* larvae at 6dpf. The black dots represent the control; gray CsA treatment ;blue LY411575; and purple combination of LY411575 and CsA. Data are presented as mean values ± SD. Two-way ANOVA with Tukey multiple comparison test, ***p-value>0.0005, ****p-value>0.00005.
E) Graph representing the mean number of mCherry+ beta cells in the pancreatic tail of *Tg(ins:NTR-P2A-mCherry) ; Tg(nkx6.1:GFP)* larvae at 5-6-7 dpf. The black dots represent the control; gray CsA treatment ;blue LY411575; and purple combination of LY411575 and CsA. Data are presented as mean values ± SEM. Two-way ANOVA test with Sidak's multiple comparison test, *p-value>0.05.

CaN controls the proliferation of duct-associated progenitors induced by Notch inhibition

Given that we observed the most significant increase in beta cell formation with CsA when Notch activity was mildly repressed (**Figure 4B-D**), and since mild Notch activity has been shown to promote progenitor amplification [35], it suggests that CaN acts at this level. To explore this possibility, we exposed briefly *Tg*(*nkx6.1:GFP*) larvae to EdU after mild Notch (LY411575 5µM) and CaN inhibition (**Figure 5A**). As expected, Notch inhibition increased the proportion of proliferating EdU+ GFP+ duct cells at 4dpf (**Figure 5B-C**) and decreased the amount of ductal progenitors 2 days later (**Figure 5D**), which is concomitant with the increase of beta cell differentiation (**Figure 4C-D**). Interestingly, the combined inhibition with CsA further increased these proportions (**Figure 5B-D**). In contrast, CaN inhibition alone had no effect on basal proliferation or on the number of ductal progenitors (**Figure 5B-D**). Incidentally, at 4dpf, while the proliferation is increased (**Figure 5C**), the number of ductal cells remained the same in all conditions (**Figure 5A supplemental**), suggesting that ductal cells have not yet left the cell cycle to differentiate. In comparison, after stronger Notch inhibition (15µM), the ductal cells are already depleted at 4dpf (**Figure 5B supplemental**), as they directly differentiate without entering the cell cycle [35]. In these conditions, CsA could therefore not enhance ductal progenitor proliferation and thus beta cell formation (**Figure 4B**). These results show that CaN and Notch pathways act together on the proliferation of the ductal progenitors to prevent their exhaustion.

CaN prevents exhaustion of Notch responsive progenitors during beta cell regeneration

Taken together, our results indicate that CaN plays a role in regulating the proliferation of ductal progenitors in contexts that are permissive for beta cell differentiation. To demonstrate that CaN regulates ductal progenitor proliferation in a similar manner to Notch inhibition but during regeneration, we exposed *Tg(ins:NTR-P2A-mCherry)*; *Tg(nkx6.1:GFP)* larvae after ablation and CsA treatment (**Figure 5E**). CaN inhibition enhanced the proliferation of ductal cells in ablated larvae (**Figure 5F-G**). To next determine if CaN acts on the Notch-responsive progenitors in beta cell regeneration, we then used *Tg(tp1:VenusPest)* Notch reporter line. At larval stages the vast majority of ductal cells are Notch responsive and the reporter line marks all the progenitors within the ductal tree [34]. We treated *Tg(ins:NTR-P2A-mCherry)*; *Tg(tp1:VenusPest)* as described above (**Figure 5E**). In ablated-larvae, CsA increased tp1+ ductal cell proliferation (**Figure 5H-I**). Moreover, CsA induced a reduction of tp1+ ductal cells in ablated larvae (**Figure 5 H-J**), suggesting an exhaustion of the Notch responsive progenitors, in accordance with premature beta cell differentiation we observed (**Figure 2B-4D**). Lastly, CsA does not affect tp1+ cells in non-ablated larvae showing that CaN inhibition did not directly affect Notch signaling (**Figure 5J**). Those results suggest that CaN fine tunes the balance between proliferation of the progenitors and their differentiation to prevent their exhaustion during beta cell regeneration.

CaN regulation is functionally relevant in adult zebrafish

To further expand upon our findings and investigate their relevance in a non-developmental context, we next ought to determine whether CaN function is maintained in older zebrafish. We used 2 months old *Tg*(*ins:NTR-P2A-mCherry*); *Tg*(*nkx6.1:GFP*) juveniles fish to perform beta cell ablation followed by CsA treatments. We analyzed the number of small islets (up to 5 cells) at 7 and 10dpt. At 7dpt, CsA increased the number of small islets in ablated larvae (**Figure 6A-B**) showing that CaN inhibition enhances beta cell regeneration in juvenile zebrafish, as in larvae. It is noteworthy that, as in larvae, we highlighted an acceleration of beta cell regeneration. The increase number of small islets is indeed transient as it not observe anymore at 10dpt (**Figure 6C**).

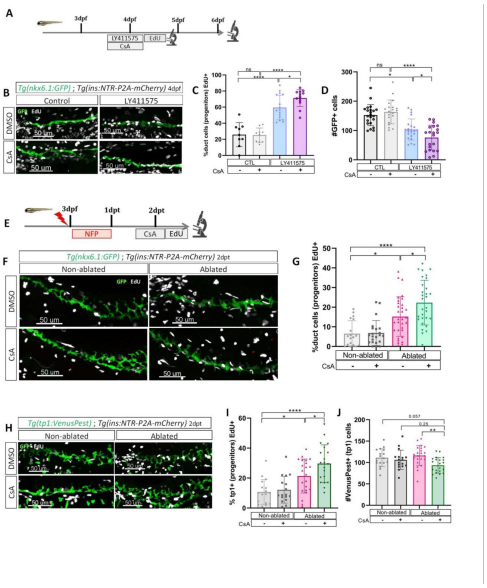

Figure 5

CaN repression increases the proportion of duct proliferating cells

A) Experimental design for EdU assay in Notch test. Larvae were treated concomitantly with LY411575 (Notch inhibitor) and CsA from 3 to 4dpf and then briefly treated with EdU before fixation and analysis at 4 dpf or at 6dpf.
B) Whole mount fluorescent immunohistochemistry (GFP and EdU) of the pancreatic tail of *Tg(ins:NTR-P2A-mCherry) ; Tg(nkx6.1:GFP)* larvae at 4dpf. 3D projection (stack) of one control (without any treatment), one with CsA only, one with LY411575 only and one with both CsA and LY411757 representative samples. Scale 50µM.
C) Barplot representing the percentage of GFP+ ductal cells which incorporated EdU+ in pancreatic tail of *Tg(ins:NTR-P2A-mCherry) ; Tg(nkx6.1:GFP)* larvae for the Notch test. The black dots represent the control; gray CsA treatment ;blue LY411575; and purple combination of LY411575 and CsA. Data are presented as mean values ± SD. T-test. Two-way ANOVA test with Tukey's multiple comparisons test, *p-value>0.05 ; ****p-value>0.00005 ; ns = non-significant.
D) Barplot representing the number of GFP+ ductal cells which in pancreatic tail of *Tg(ins:NTR-P2A-mCherry) ; Tg(nkx6.1:GFP)* larvae at 6dpf for the Notch test. The black dots represent the control; gray CsA treatment ;blue LY411575; and purple combination of LY411575 and CsA. Data are presented as mean values ± SD. T-test. Two-way ANOVA test with Tukey's multiple comparisons test, *p-value>0.05 ; ****p-value>0.00005 ; ns = non-significant.
E) Experimental design for EdU assay in regeneration. Larvae were treated with nifurpirinol for beta cell ablation from 3 to 4dpf then with CsA from 4 to 5dpf and then briefly treated with EdU before fixation and analysis.
F) Whole mount fluorescent immunohistochemistry (GFP and EdU) of the pancreatic tail of *Tg(ins:NTR-P2A-mCherry) ; Tg(nkx6.1:GFP)* larvae at 5dpf. 3D projection (stack) of one representative sample of non-ablated or ablated with or without CsA are shown. Scale 50µM.
G) Barplot representing the percentage of GFP+ ductal cells which incorporated EdU+ in pancreatic tail of *Tg(ins:NTR-P2A-mCherry) ; Tg(nkx6.1:GFP)* larvae at 5dpf. The gray spheres represent non-ablated condition ; the pink triangles the ablated condition ; the black squares CsA condition and inverted green triangles ablated + CsA condition. Data are presented as mean values ± SD. Two-way ANOVA test with Tukey's multiple comparisons test, *p-value>0.05 ; ****p-value>0.00005 ; ns = non-significant.
H) Whole mount fluorescent immunohistochemistry (VenusPest and EdU) of the pancreatic tail of *Tg(ins:NTR-P2A-mCherry) ; Tg(tp1:VenusPest)* larvae at 5dpf. 3D projection (stack) of one representative sample of non-ablated or ablated with or without CsA are shown. Scale 50µM.
I) Barplot representing the percentage of GFP+ ductal cells which incorporated EdU+ in pancreatic tail of *Tg(ins:NTR-P2A-mCherry) ; Tg(tp1:VenusPest)* larvae at 5dpf. The gray spheres represent non-ablated condition ; the pink triangles the ablated condition ; the black squares CsA condition and inverted green triangles ablated + CsA condition. Data are presented as mean values ± sd. Two-way ANOVA test with Tukey multiple comparisons test, *p-value>0.05 ; ****p-value>0.00005 ; ns means non-significant.
J) Barplot representing the number of VenusPest+ ductal cells which incorporated EdU+ in pancreatic tail of *Tg(ins:NTR-P2A-mCherry) ; Tg(tp1:VenusPest)* larvae at 5dpf. The gray spheres represent non-ablated condition ; the pink triangles the ablated condition ; the black squares CsA condition and inverted green triangles ablated + CsA condition. Data are presented as mean values ± SD. Two-way ANOVA test with Tukey's multiple comparisons test, **p-value>0.005.

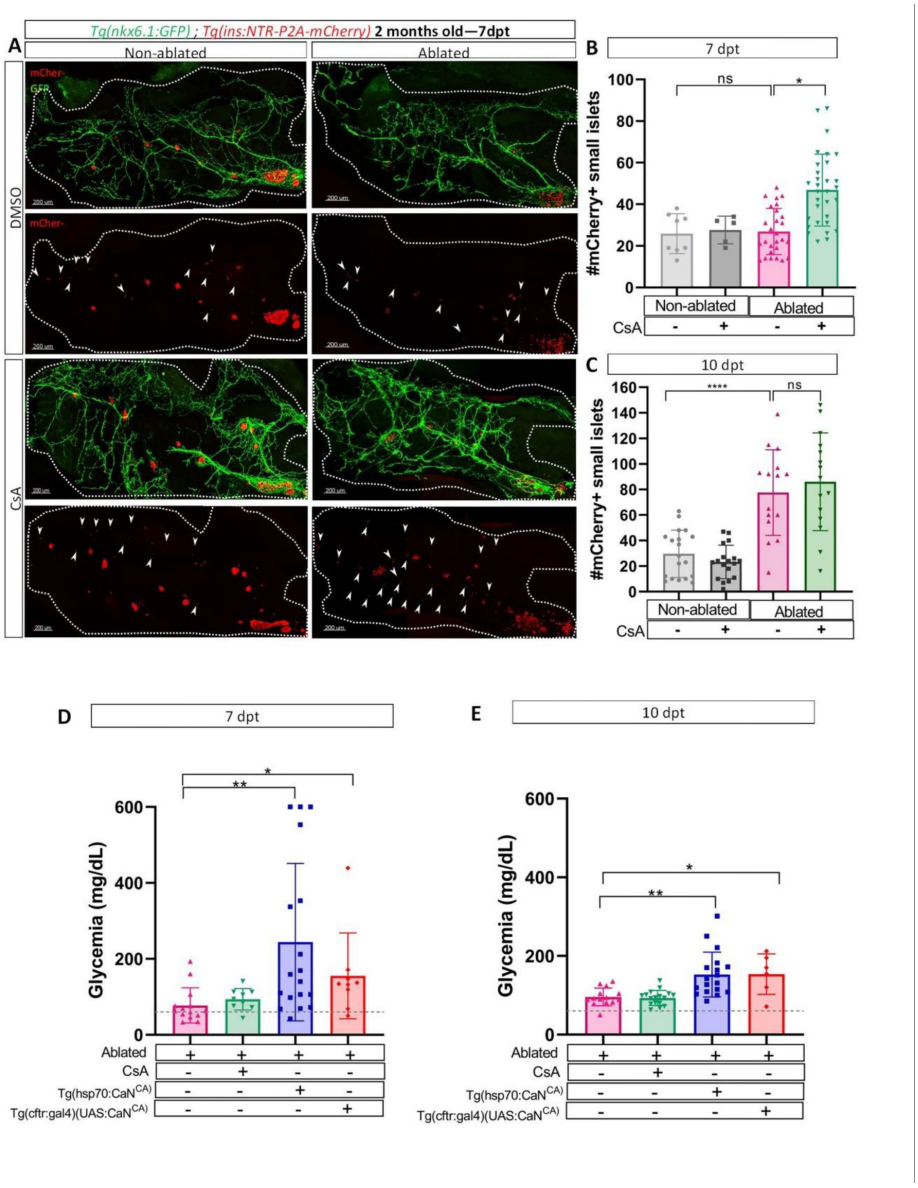

Figure 6

CaN regulation is important in juveniles/adults and necessary for correct glycemia recovery

A) Whole mount fluorescent immunohistochemistry (GFP and mCherry) of the pancreas of *Tg(ins:NTR-P2A-mCherry) ; Tg(nkx6.1:GFP)* 2 months old zebrafish at 7dpt. 3D projection (stack) of non-ablated and ablated larvae treated with DMSO or CsA representative samples. The principal islet (PI) and the pancreatic tail are shown. Arrows point out mCherry+ beta cells in the pancreatic tail. Scale 200µM

B-C) Barplot representing the number of number of mCherry+ small secondary islets (=<5 cells) in the pancreatic tail of *Tg(ins:NTR-P2A-mCherry) ; Tg(nkx6.1:GFP)* 2 months old zebrafish at 7 **(B)** and 10dpt **(C).** The gray spheres represent non-ablated condition ; the pink triangles represent the ablated condition ; the black squares CsA condition and inverted green triangles ablated + CsA condition. Data are presented as mean values ± SD. Two-way ANOVA with Tukey's multiple comparison test, *p-value>0.05.

D-E) Barplot representing the glycemia (mg/dL) of *Tg(ins:NTR-P2A-mCherry) ;* months old adult zebrafish at 7 **(D)** and 10dpt **(E).** The pink triangles represent the ablated condition ; the inverted green triangles ablated + CsA condition; the blue squares *Tg(hsp70:CaN^{CA})* after heat shocks ; the orange lozenges *Tg(UAS:CaN^{CA})*; *Tg(cftr:gal4)*. The grey line represents the mean glycemia of controls (non-ablated) fish. Data are presented as mean values ± SD. One-way ANOVA with Tukey's multiple comparison test, *p-value>0.05; **p-value>0.005.

Next, we determined the functional impact of CaN overexpression or inhibition by assessing the glycemia at 7, 10 and 14 after beta cell ablation. Overexpression of CaN^{CA} using either *Tg(hsp70:GFP-P2A-ppp3cc*^{CA}*)* or *Tg*(*cftr:gal4*); *Tg*(*UAS:GFP-P2A-ppp3cc*^{CA}*), led to an increased glycemia at both 7 and 10dpt* (**Figure 6D-E**), before recovery at 14 dpt (**Figure 6A supplemental**). This indicates that the overexpression of CaN impedes the recovery of glycemia induced by beta cell regeneration. However, CaN inhibition did not seem to further improve the glycemia (**Figure 6D-E**) probably because the glycemia was already low at 7dpt (77 mg/dL on average) compared to non-ablated control (mg/dl) (**Figure 6D-E**). Altogether, these results show that in adult zebrafish also, CaN regulation is necessary to enable beta cell regeneration and for proper recovery of the glycemia after beta cell loss.

Discussion

The present study reveals the importance of the protein phosphatase CaN as a new player in beta cell regeneration in zebrafish. We demonstrate that CaN act on ductal-associated progenitor cells by balancing proliferation and endocrine differentiation. In addition, we show the interplay between CaN and Notch signalling, a master regulator of beta cell regeneration.

Previous drug and genetic screening using zebrafish larvae enabled the identification of several regulators of beta cell regeneration from different pancreatic cellular sources. For example, adenosine has been shown to stimulate beta cell replication [28] and, igfbp1a [42] and TGFb suppression [30] promote alpha-to-beta cell transdifferentiation. As for cdk5 inhibition and folinic acid/Folr1, they promote beta cell regeneration from the pancreatic ducts [43], [44]. Here, to identify novel regulators of beta cell regeneration specifically from pancreatic ducts, we carried out a transcriptomic profiling of duct cells following beta cell ablation in the adult zebrafish. Transcriptomic analyses show that the regulated genes encompass most of the genes and pathways identified in previous studies (igfbp1, mTor, Notch, etc.), underlying the importance of those actors in beta cell regeneration. Our data reveal also that DNA replication is the most enriched signature attesting that duct cells undergo a potent proliferative response after the destruction of beta cells.

Besides these expected signatures, our transcriptomic data uncover the unanticipated upregulation of numerous genes implicated in DNA repair and cell cycle arrest. These signatures might indicate that highly proliferating ductal cells activate counteracting mechanisms. Among the genes regulated in those signatures, we focused on CaN and determined its role in beta cell regeneration. Pharmacological inhibition of CaN increases the proliferation of duct cells induced by beta cell ablation, resulting in an acceleration of beta cell regeneration in the ducts. Consistently, transgene-mediated CaN overactivation abolishes the regenerative response. Importantly, the inhibition of regeneration is observed when CaN is overexpressed either ubiquitously or selectively in *cftr*-expressing ductal cells indicating that the role of CaN in beta cell regeneration is intrinsic to the ducts. Based on functional assays in larvae, we not only confirm the activation of the proliferation of ductal cells soon after beta cell ablation, but also that the rate of progenitor proliferation is carefully controlled by CaN in order to achieve proper and timely regeneration of beta cells. Our data are consistent with earlier studies reporting a role of CaN in proliferation dynamics during fin regeneration. In the regenerating fin, low CaN activity is found in the proximal region of the blastema characterized by a high rate of proliferation and regeneration and its activity increases distally where lower proliferation is observed [36], [38], [39]. It was suggested that CaN control blastemal cell progeny divisions [36]. In human, the importance of CaN in proliferation is also highlighted in organ transplanted patients. When patients are treated with Cyclosporin A (*i.e.* the CaN inhibitor we used in this study) as immunosuppressive drug they indeed present an increased risk of skin cancer, notably due to keratinocyte senescence inhibition [45].

It has been shown that Notch inhibitory treatments switch progenitors from proliferative self-renewing to premature differentiation, leading to progenitor depletion [34], [35]. Our study reveals that this phenomenon is further exacerbated by CaN inhibition. Importantly, during normal larval development in absence of Notch inhibitory treatment, CaN does not affect basal ductal proliferation nor beta cell differentiation. Hence, Notch signalling has to be repressed to detect the effect of CaN on the progenitors, suggesting that CaN acts downstream of Notch pathway. In differentiating keratinocytes, CaN cooperates with Notch signalling to regulate p21/*cdkn1a* (which is upregulated in the ducts at 3 dpt), cell cycle withdrawal and differentiation [46]. These studies show that CaN acts in association with Notch signalling on progenitors proliferation and on their differentiation.

Based on our data, we build the model depicted in **Figure 7A**. Our study suggests that CaN acts in competent progenitor cells and that this competence is determined by Notch signalling. When Notch is repressed to a mild level, the progenitor enter into the cell cycle and acquire a pro-endocrinogenic competence [35]. CaN acts on these progenitors to tone down an excessive proliferation and avoid the exhaustion of these progenitors. CaN is therefore a guardian of the progenitor population. CaN inhibition both increases progenitor proliferation and induces their depletion, suggesting a switch to a symmetric division resulting in two daughter cells entering in endocrine differentiation.

More precisely, a previous study in mice uncover the existence of three division modes of the pancreatic progenitors during embryonic development, *i.e.* symmetric self-renewing resulting in two progenitors cells ; asymmetric resulting in a progenitor and a endocrine cell and symmetric differentiative resulting in two differentiated cells [47]. The authors actually show that the type of division is defined by the timing of induction of endocrine program by NEUROG3 [47]. Interestingly, NEUROG3 seems to be the link between proliferation and differentiation, and its expression is regulated by Notch signalling [48]. In zebrafish, endocrine differentiation is not induced by *Neurog3* but by *Ascl1b* and *Neurod1* [49]. Concerning that subject, CaN inhibition accelerates the formation of neurod1+ cells. Hence CaN could possibly act via the determination of the type of division *i.e.* symmetric vs asymmetric. This model is supported by previous observation in others systems. In stem cells and neuronal and hematopoietic progenitors, premature differentiation results from a switch in the mode of cellular division, from symmetric amplifying division to asymmetric differentiating division [50], [51]. Notch determines the choice between both types of divisions [52], [53].

Calcineurin is known to be implicated in cellular senescence [45]. Usually thought as negative regulators of development and cellular growth, DNA repair [54] and cellular senescence [55] appear to be required in both developmental and regenerative processes. Our transcriptomic data suggest that these mechanisms are required for beta cell regeneration. Therefore, it would be interesting to determine the contribution of these cellular processes in the ductal progenitors and determine if CaN acts via cellular senescence in this case.

Overall, this study brings new insights on beta cell regeneration and highlights the ductal progenitor cell cycle as a cornerstone in the process. Some studies report an increase of proliferation of some ductal cell population in diabetic patients [10], [56], implying a regenerative response. However, these ductal cells cannot efficiently reform the beta cell mass, suggesting a dormant mechanism of regeneration. As such, the balance between proliferation and induction of endocrine differentiation could be a key to improve beta cell neogenesis. However, as CaN is also important for beta cell function, this approach would require to be transient to induce neogenesis. Therefore, it should be combined with methods to induce beta cell proliferation to ultimately reconstitute the beta cell mass. Overall, this study brings a better understanding on the regulation of the balance between ductal progenitors proliferation and endocrine differentiation. These results should provide new hints to help improve regenerative competences in mammals.

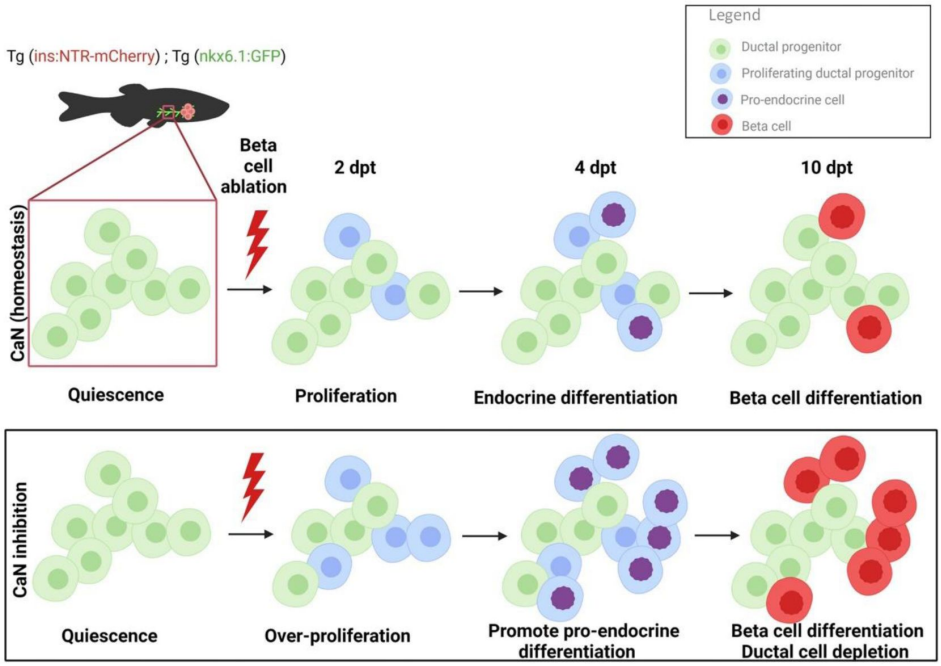

Figure 7

Model of CaN action on ductal progenitors to regenerate beta cells

A) Under physiological conditions, the behavior of the ductal progenitors is determined by Notch signaling. Calcineurin is active in these progenitors and enable a proper control between proliferation and differentiation. When CaN in repressed, more ductal progenitors enter in the cell cycle (2dpt) and switch to a mode of proliferation leading to differentiation of the two daughter cells (4dpt), as more pro-endocrine cells are formed. The result is a exhaustion of the progenitors and a premature beta cell differentiation (10dpt).

Material and Methods

Key resources table

Reagent type or resource	Designation	Source or reference	Identifier	Additional information
Genetic reagent (Danio rerio)	*TgBAC(nkx6.1:eGFP)^{ulg004}*	PMID: 26329351	ZFIN: ZDB-ALT-160205-1	
Genetic reagent (Danio rerio)	*Tg(ins:NTR-P2A-mCherry)^{ulg034}*	PMID: 29663654	ZFIN: ZDB-ALT-171122-9	
Genetic reagent (Danio rerio)	*Tg(cftr:gal4)*	PMID: 25592226	ZFIN : ZDB-FISH-150901-25442	
Genetic reagent (Danio rerio)	*Tg(tp1:VenusPest)*	PMID: 22492351	ZFIN: ZDB-FISH-150901-8023	
Genetic reagent (Danio rerio)	*Tg(hsp70:eGFP-P2A-ppp3ccaCA) ^{ulg068}*	This paper		See Zebrafish husbandry and generation of the *Tg(hsp70:eGFP-P2A-ppp3ccaCA) zebrafish line*
Genetic reagent (Danio rerio)	*Tg(UAS:eGFP-P2A-ppp3ccaCA) ^{ulg069}*	This paper		See Zebrafish husbandry and generation of the *Tg(UAS:eGFP-P2A-ppp3ccaCA) zebrafish line*
Antibody	Anti-GFP (chicken polyclonal)	Aves Labs	GFP-1020	1:1000
Antibody	anti-mCherry/dsRed (Living Colors Polyclonal)	Clontech	632496	1:500
Antibody	Anti-glucagon (mouse polyclonal)	Sigma	G2654	1:300
Antibody	Goat anti-Chicken IgY (H+L), Alexa Fluor™ 488	Invitrogen	A-11039	1:750
Antibody	Goat anti-dsred 568	Invitrogen		1:750

Antibody	Goat anti-Mouse IgG (H+L) Cross-Adsorbed Secondary Antibody, Alexa Fluor 633	Invitrogen		1:750
Chemical compound	Nifurpirinol (NFP)	Sigma-Aldrich	32439	
Chemical compound	Metronidazole (MTZ)	Sigma-Aldrich	M1547	
Chemical compound	Cyclosporine A (CsA)	Selleckchem	S2286	
Chemical compound	LY411575	Sigma-Aldrich	SML0506	
Chemical compound	CHIR990211	Sellekchem	CT99021	
Commercial assay or kit	Gateway™ LR Clonase™ II Enzyme mix	Invitrogen	11791020	
Commercial assay or kit	Gateway™ BP Clonase™ II Enzyme mix	Invitrogen	11789020	
Sequence based reagent	IM369	This paper	PCR primer	gaagaaaaccccggtcctatgtc gacgaaagagccgaaag
Sequence based reagent	IM380	This paper	PCR primer	ccttacacattcccgtcagtgc
Sequence based reagent	IM371	This paper	PCR primer	CGGCTCTTTCGTCGACAT AGGACCGGGGTTTTCTTC CACG
Sequence based reagent	O226	This paper	PCR primer	GCCACCATGGTGAGCAA GGGCGAGGA
Sequence based reagent	IM370	This paper	PCR primer	ttattagatcttatttctgatcacc tcctt
Sequence based reagent	IM459	This paper	PCR primer	cacacgaattcgccgccaccAT GGTGAGCAAGGGCGAG
Sequence based reagent	IM460	This paper	PCR primer	ggatcggtcgagatccttacGA TCTTATTTCTGATCACCTC CTTACG
Sequence based reagent	IM457	This paper	PCR primer	GTAAGGATCTCGACCGAT CCTG
Sequence based reagent	IM458	This paper	PCR primer	GGTGGCGGCGAATTCGT G
Commercial assay or kit	Nextera® XT DNA Library kit	Illumina	FC-131-1024	
Commercial assay or kit	Click-iT™ EdU Cell Proliferation Kit for Imaging, Alexa Fluor™ 647 dye	Invitrogen	C10340	

Software, algorithm	Imaris	Bitplane (http://www.bitplane.com/imaris/imaris)	RRID:SCR_007370	Version 9.5
Software, algorithm	GraphPad Prism	GraphPad Prism (https://graphpad.com)	RRID:SCR_015807	Version 8
Software, algorithm	DESeq2	DESeq2 (https://bioconductor.org/packages/release/bioc/html/DESeq2.html)	RRID:SCR_015687	
Software, algorithm	WebGestalt	WebGestalt (http://www.webgestalt.org/)	RRID:SCR_006786	

Zebrafish husbandry and generation of the Tg(hsp70:eGFP-P2A-ppp3ccaCA)^{ulg068} and Tg(UAS:eGFP-P2A-ppp2ccaCA)^{ulg069} zebrafish lines

Tg BAC(nkx6.1:eGFP)^{ulg004} [57] *; Tg(ins:NTR-P2A-mCherry)*^{ulg034} [58] *; Tg(cftr:gal4)* and *Tg(tp1:VenusPest)* were used. Zebrafish were raised in standard conditions at 28°C. All experiments were carried out in compliance with the European Union and Belgian law and with the approval of the ULiège Ethical Committee for experiments with laboratory animals (approval number : 2075).

The *hsp70:GFP-P2A-ppp3ccaCA* transgene has been generated by cloning a PCR fragment containing the Gateway vector pCR8/GW/TOPO. Firstly, we amplified the full length of ppp3ccaCA with primers IM369/IM380 and amplified *GFP-P2A* with overlapping regions with IM371/O226. The overlapping PCR used the primers O226/IM380. Then to obtain a truncated *ppp3ccaCA* lacking the calmodulin biding and the autoinhibitory domain, resulting in a constantly active form of calcineurin, we amplified the last fragments with IM370/O226 and cloned into PCR8 vector. The promoter was assembled by LR recombination with pE5-hsp70 into pDestTol2p2A from the Tol2kit [59]. *Tg (hsp70:GFP-P2A-ppp3ccaCA)* fish have been generated using the Tol2 mediated transgenesis [60]. *The Tg(UAS:GFP-P2A-ppp3ccacA*) has been generated by ligation (KLD kit, NEB) of PCR fragments *GFP-P2A-ppp3ccacA (*IM459/IM460) with the UAS sequences (IM457/IM458) in plasmid from (Distel 2009) and then inserted into pDestTol2p2A from the Tol2kit. Final constructions has been injected with transposase into wild type (WT) AB embryos.

Beta-cell ablation

Adults fish for RNA-sequencing experiment were treated with freshly prepared metronidazole (MTZ) (Sigma M1547) at 10mM with 0.2% DMSO in fish water. Control treatments consisted of fish water containing 0.2% DMSO. Fish were treated for 18 hours in the dark. Nifurpirinol (NFP) (32439, Sigma-Aldrich) stock solution was dissolved at 2.5 mM in DMSO. b-cell ablation in *Tg(nkx6.1:eGFP); Tg(ins:NTR-P2A-mCherry)* larvae was induced by treatment with 2.5 µM NFP in E3. Control treatments consisted of E3 containing 0.2% DMSO. Larvae were treated for 18 hours in the dark.

Drug treatments

Cyclosporine A (Selleckchem, S2286), CHIR99021 and LY411575 (Sigma-Aldrich, SML0506) stock solution were dissolved at 10mM in DMSO. Larvae treatment were respectively performed at 0.1 µM and 5µM in E3. Control treatments consisted of E3 containing the same amount of DMSO than drug treatment. Larvae were treated for 18 hours in the dark.

5-ethynyl-2'-deoxyuridine (EdU) incorporation assay

Zebrafish larvae were incubated in 4 mM EdU dissolved in E3 water for 8 hours, they were then directly euthanised in tricaine and fixed in 4% PFA. EdU was detected according to the protocol of Click-iT™ EdU Cell Proliferation Kit for Imaging, Alexa Fluor™ 647 (ThermoFisher C10340) after whole mount immunodetection.

Heat Shock

Successive heat shocks of 30 minutes and 12 hours apart were performed at 39°C for larvae and 37°C for juveniles and adults zebrafish.

Whole mount immunodetection

Larvae were euthanized in tricaine and fixed in 4% PFA at 4 °C for IHC. The digestive tract of juveniles was dissected prior immunodetection and kept in methanol for at least 18 hours. After depigmentation with 3% H2O2/1% KOH, larvae were permeabilised 30 min in PBS/ Triton X-100 and incubated for two hours in blocking buffer (4% goat serum/1% BSA/PBS/0.1% Triton X-100). Primary and secondary antibodies were incubated at 4 °C overnight.

	Fixation duration	Depigmentation duration	Permeabilization solution	Permeabilization duration
5-10 dpf	18 hours	15 min	PBTr 0.05%	30 min
13-17 dpf	36 hours	20 min	PBTr 2%	30 min
2months (digestive tract)	18 hours	15 min	/	/

Primary antibodies: Living Colors Polyclonal anti-mCherry/dsRed (rabbit, 1:500, Clontech 632496), anti-GFP (chicken, 1:1000), Secondary antibodies: Alexa Fluor-488,-568,-633 (goat, 1:750, Molecular Probes).

Flow cytometry and FACS

The whole pancreas from 3-4 fish of *Tg(nkx6.1:eGFP); Tg(ins:NTR-P2A-mCherry)* adult fish (6–10 months old, males and females) were dissected, collected and washed in HBSS without Ca^{2+}/Mg^{2+}. Live cell dissociation was performed in Tryple Select 1x solution (GIBCO) supplemented with 100 U/mL collagenase IV (Life Technologies 17104-019) and 40 µg/mL proteinase K (Invitrogen, 25530031) for 10 min at 28 °C.

The GFP+ cells were selected on FACS Aria III and sorted under purity mode and after exclusion of the doublets. The purity of the sorted cells was confirmed by epifluorescence microscopy (~95 %). Cells (about 1000-5000/fish depending on the cell type) were immediately lysed with 0.5% Triton X-100 containing 2U/µl RNAse inhibitor and stored at –80 °C.

mRNA sequencing of FACSed cells and bioinformatic analyses

cDNAs were prepared from lysed cells according to SMART-Seq2.0 (Picelli et al., 2014) for low input RNA sequencing and libraries were prepared with Nextera® DNA Library kit (Illumina). Independent biological replicates of each cell type sequenced using Illumina NextSeq500 and obtained ~20 million 100 bp paired-end reads. Reads were mapped and aligned to the zebrafish genome GRCz11 from Ensembl gene annotation version using STAR version 2.6.1 (Dobin et al., 2013). Gene expression levels were calculated with featureCounts

(*http://bioinf.wehi.edu.au/featureCounts/*) and differential expression determined with DESeq2 (Love, Huber, & Anders, 2014). Expression values are given as normalized read counts. Poorly expressed genes with mean normalized expression counts <10 were excluded from the subsequent analyses. DESeq2 uses Wald test for significance with posterior adjustment of P values (Padj) using Benjamini and Hochberg multiple testing. The differentially expressed (DE) genes identified with a Padj cutoff of 0.05 were submitted for GO analysis using WebGestalt tool (Liao, Wang, Jaehnig, Shi, &Zhang, 2019).

Confocal microscopy and image analysis

Images were acquired using Leica SP5 confocal microscope. We used ImageJ to count the cells and Imaris to do the pictures.

Glycemia measurement

Glycemia measurement were performed as described in [58].

Data availability

The sequences that support the findings are of this study have been deposit in Geo with the accessions codes GSE212124, *https://www.ncbi.nlm.nih.gov/geo/info/linking.html*. The authors declare that all other data supporting the findings of this study are available within the paper and its supplementary information files.

Authors contribution

L.M. conducted experiments, acquired and analysed data, analysed transcriptomic data, wrote the manuscript. **D.B.** conducted RNA-seq experiment and revised the manuscript **A.L.** implemented bioinformatic programs and analysed transcriptomic data. **C.R., C.G. and C.D.** conducted experiments. **L.F.** revised the manuscript. **B.P.** provided resources and advised on research studies. **M.L.V.** provided resources, advised on research studies and revised the manuscript **I.M.** supervised the whole work, acquired funding, designed the research studies, verified data and assisted in writing the manuscript.

Acknowledgements

The authors thank the GIGA technology platforms GIGA-Genomics and GIGA-Imaging. The authors also thanks Jérémie Zappia for critically reading the manuscript, Jordane Bourdouxhe and Marie Alice Dupont for their help with the constructions.

Duality of interest

No potential conflicts of interest.

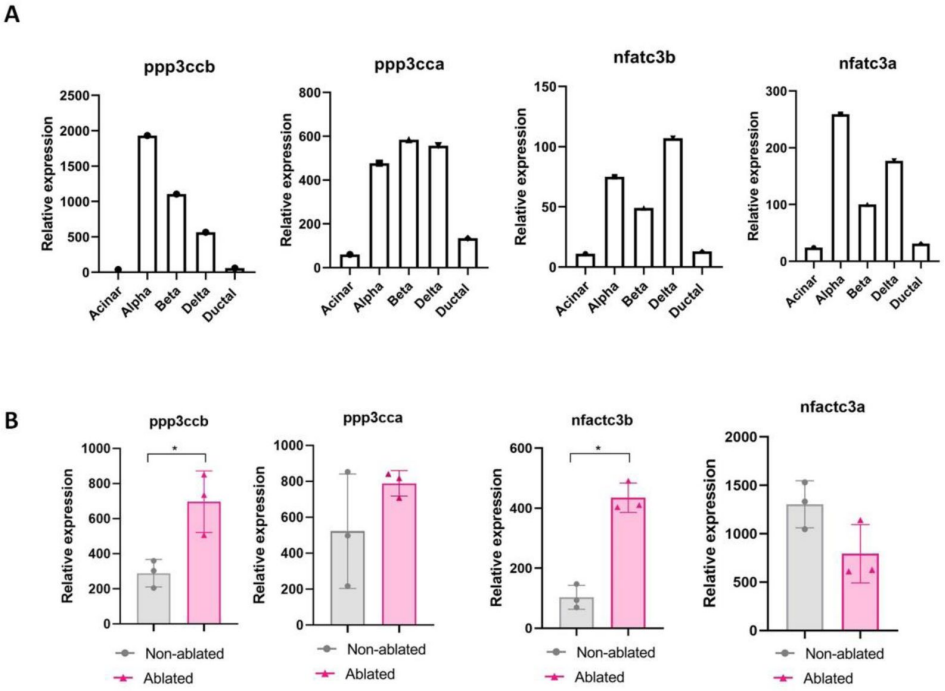

Figure 1 supplemental

Transcriptomic profiling of ductal cells during beta cell regeneration and validation in larvae

A) Expression of *ppp3cca; ppp3ccb ; nfatc3a ; nfatc3b* in acinar, alpha, beta, delta or ductal cells population from the zebrafish pancreas [40].
B) Calcineurin (*ppp3ccb and ppp3cca)* and NFATc3 (*nfatc3a and nfatc3b)* expression in ductal cells from zebrafish in non-ablated and ablated conditions.

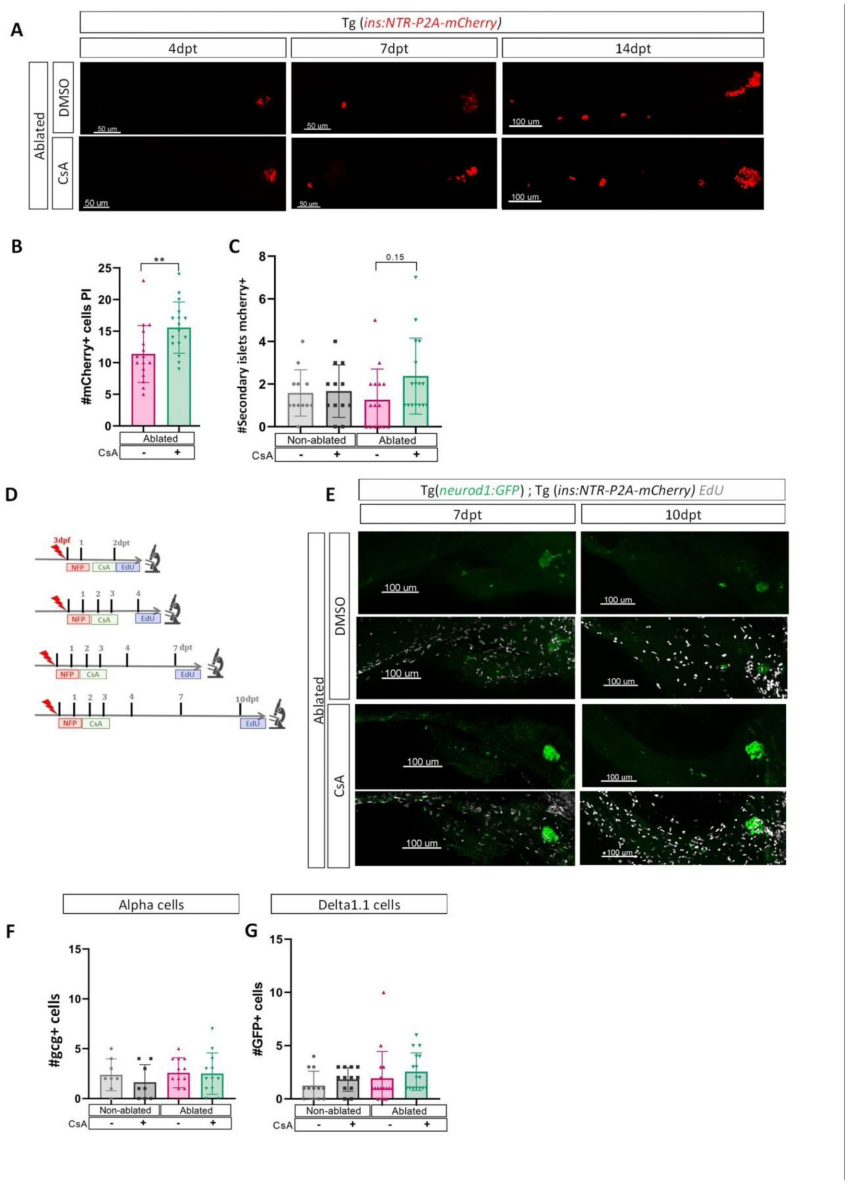

Figure 2 supplemental

Calcineurin inhibition with CsA increases the ductal regenerative response

A) Whole mount fluorescent immunohistochemistry (mCherry) of the pancreas of *Tg(ins:NTR-P2A-mCherry)* larvae at 4-7 and 14dpt. 3D projection (stack) of ablated larvae treated with DMSO or CsA representative samples. The principal islet (PI) and the pancreatic tail are shown. Scale 50 or 100µM.
B-C) Barplot representing the number of mCherry+ beta cells in the principal islet (PI) **(B)** and the number of secondary islets of mCherry+ beta cells in the pancreatic tail **(C)** of Tg(ins:NTR-P2A-mCherry) ; Tg(nkx6.1:GFP) larvae at 10dpt. Data are presented as mean values ± SD. T-test or Two-way ANOVA with Tukey's multiple comparison test. **p-value>0.005
D) Experimental design for EdU assay in larvae. After NFP treatment for 3 to 4dpf, larvae were exposed to EdU before fixation for analysis.
E) Whole mount fluorescent immunohistochemistry (GFP and EdU) of the pancreas of Tg(ins:NTR-P2A-mCherry) ; Tg(neurod1:GFP) larvae at 2-4-7 and 10 dpt. 3D projection (stack) of non-ablated and ablated larvae treated with DMSO or CsA representative samples. The principal islet (PI) and the pancreatic tail are shown. Scale 50µM.
F-G) Barplot representing the number of gcg+ alpha cells **(F)**; the number of GFP+ sst1.1 delta cells **(G);** of Tg(*ins:NTR-P2A-mCherry*) ; Tg(*sst1.1:GFP*) larvae at 10dpt. Gcg was detected by IHC. The gray spheres represent non-ablated condition ; the pink triangles represent the ablated condition ; the black squares CsA condition and inverted green triangles ablated + CsA condition. Data are presented as mean values ± SD. Two-way ANOVA with Tukey's multiple comparison test. **p-value>0.005

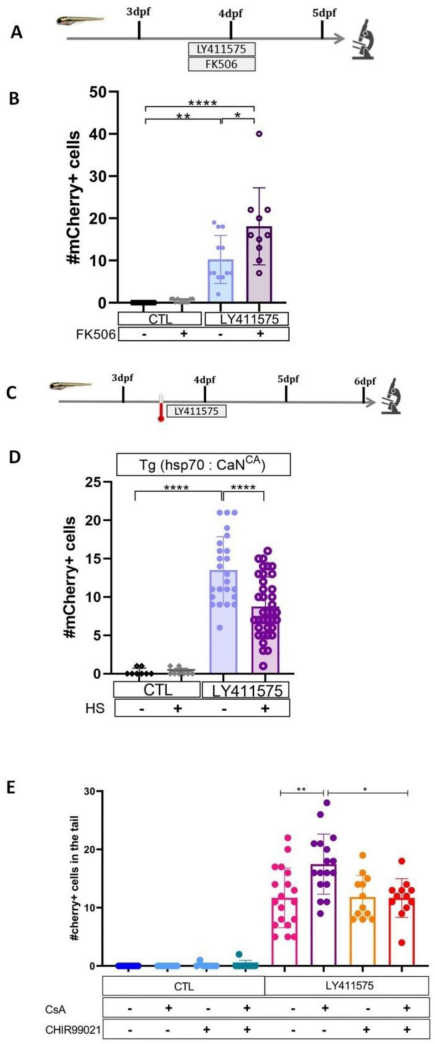

Figure 4 supplemental

CaN repression potentializes the effect of Notch inhibition on beta cell formation

A) Experimental design for Notch inhibition test in non-ablated condition. Larvae were treated concomitantly with LY411575 (Notch inhibitor) and FK506 from 3 to 4dpf and were fixed and analyzed at 5dpf.
B) Barplot representing the mean number of mCherry+ beta cells in the pancreatic tail of *Tg(ins:NTR-P2A-mCherry) ; Tg(nkx6.1:GFP)* larvae at 5dpf. The black dots represent the control; gray FK506 treatment ;blue LY411575; and purple combination of LY411575 and FK506. Data are presented as mean values ± SD. Two-way ANOVA with Tukey multiple comparison test, *p-value>0.05,**p-value>0.005, ****p-value>0.00005.
C) Experimental design for Notch inhibition test in non-ablated condition. Larvae were heat-shocked and then directly treated with LY411575 (Notch inhibitor) from 3 to 4dpf and were fixed and analyzed at 6dpf.
D) Barplot representing the mean number of mCherry+ beta cells in the pancreatic tail of *Tg(hsp70:CaN^{CA})*; *Tg(ins:NTR-P2A-mCherry) ; Tg(nkx6.1:GFP)* larvae at 5dpf. The black dots represent the control; gray heat-shock ;blue LY411575; and purple combination of LY411575 and heat-shock. Data are presented as mean values ± SD. Two-way ANOVA with Tukey multiple comparison test, ****p-value>0.00005.
E) Barplot representing the mean number of mCherry+ beta cells in the pancreatic tail of *Tg(ins:NTR-P2A-mCherry) ; Tg(nkx6.1:GFP)* larvae at 6dpf after Notch inhibition (LY411575), CaN inhibition (CsA) and NFATc inhibition (CHIR99021). Data are presented as mean values ± SD. Two-way ANOVA with Tukey multiple comparison test, *p-value>0.05,**p-value>0.005, ****p-value>0.00005.

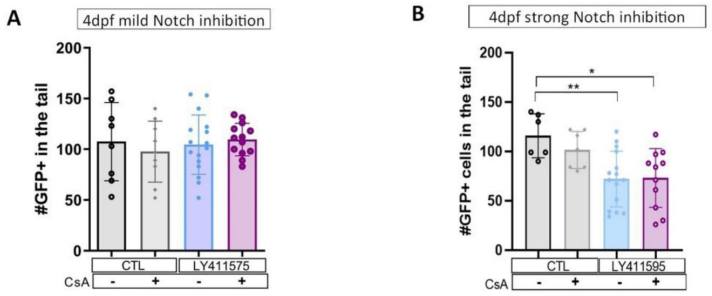

Figure 5 supplemental

CaN repression increases the proportion of duct proliferating cells

A-B) Barplot representing the number of GFP+ ductal cells which in pancreatic tail of *Tg(ins:NTR-P2A-mCherry) ; Tg(nkx6.1:GFP)* larvae at 4dpf for the Notch test. **(A)** Mild Notch inhibition with LY411575 5µM and **(B)** stronger Notch inhibition with LY411575 15µM. The black dots represent the control; gray CsA treatment ;blue LY411575; and purple combination of LY411575 and CsA. Data are presented as mean values ± SD. T-test. Two-way ANOVA test with Tukey's multiple comparisons test, *p-value>0.05 ; ****p-value>0.00005 ; ns = non-significant.

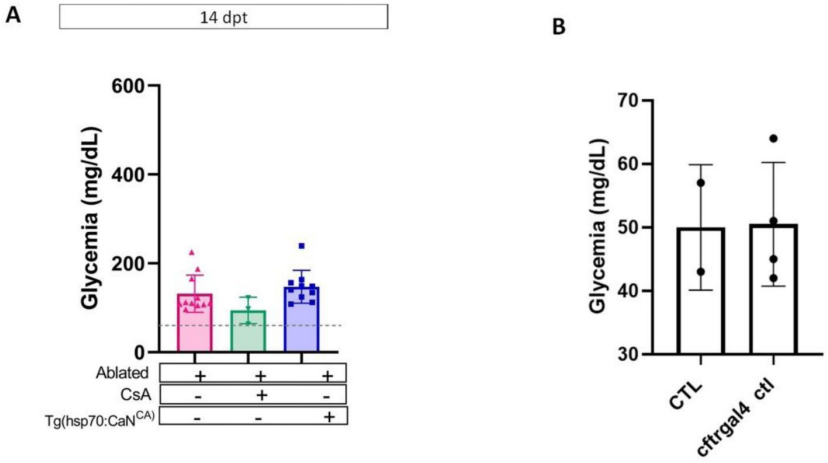

Figure 6 supplemental

CaN regulation is important in juveniles/adults and necessary for correct glycemia recovery

A) Barplot representing the glycemia (mg/dL) of *Tg(ins:NTR-P2A-mCherry) ;* months old adult zebrafish at 14dpt**.** The pink triangles represent the ablated condition ; the inverted green triangles ablated + CsA condition; the blue squares *Tg(hsp70:CaN^{CA})* after heat shocks. The grey line represents the mean glycemia of controls (non-ablated) fish. Data are presented as mean values ± SD.

B) Barplot representing the glycemia (mg/dL) of *Tg(ins:NTR-P2A-mCherry) ; and Tg(UAS:CaN^{CA}); Tg(cftr:gal4)* in non-ablated adult zebrafish. Data are presented as mean values ± SD.

References

[1] Dor Y., Brown J., Martinez O. I., a Melton D. (1970) **Adult pancreatic beta-cells are formed by self-duplication rather than stem-cell differentiation** *Nature* **429**:41–46 https://doi.org/10.1038/nature02520

[2] Thorel F., et al. (2010) **Conversion of Adult Pancreatic alpha-cells to Beta-cells after Extreme Beta Cell Loss** *Nature* **464**:1149–1154 https://doi.org/10.1038/nature08894.Conversion

[3] Chera S., et al. (2014) **Diabetes recovery by age-dependant conversion of pancreatic delta-cells into insulin producers** *Nature* **514** https://doi.org/10.1038/nature13633.Diabetes

[4] Xu X., et al. (2008) **Beta Cells Can Be Generated from Endogenous Progenitors in Injured Adult Mouse Pancreas** *Cell* **132** https://doi.org/10.1016/j.cell.2007.12.015

[5] Solar M., et al. (2009) **Pancreatic Exocrine Duct Cells Give Rise to Insulin-Producing β Cells during Embryogenesis but Not after Birth** *Dev. Cell* **17** https://doi.org/10.1016/j.devcel.2009.11.003

[6] Zhao H., et al. (2021) **Pre-existing beta cells but not progenitors contribute to new beta cells in the adult pancreas** *Nat. Metab* **3** https://doi.org/10.1038/s42255-021-00364-0

[7] Kopp J. L., et al. (2011) **Sox9+ ductal cells are multipotent progenitors throughout development but do not produce new endocrine cells in the normal or injured adult pancreas** *Development* **138**

[8] Courtney M., et al. (2013) **The Inactivation of Arx in Pancreatic α-Cells Triggers Their Neogenesis and Conversion into Functional β-Like Cells** *PLoS Genet* **9** https://doi.org/10.1371/journal.pgen.1003934

[9] Gribben C., et al. (2021) **Ductal Ngn3-expressing progenitors contribute to adult β cell neogenesis in the pancreas** *Cell Stem Cell* **28**:2000–2008 https://doi.org/10.1016/j.stem.2021.08.003

[10] Qadir M. M. F., et al. (2020) **Single-cell resolution analysis of the human pancreatic ductal progenitor cell niche** *Proc. Natl. Acad. Sci. U. S. A* **117** https://doi.org/10.1073/pnas.1918314117

[11] Moss J. B., Koustubhan P., Greenman M., Parsons M. J., Walter I., Moss L. G. (1970) **Regeneration of the pancreas in adult zebrafish** *Diabetes* **58**

[12] Poss K. D., Wilson L. G., Keating M. T. (1970) **Heart regeneration in zebrafish** *Science*

[13] Choi T. Y., Ninov N., Stainier D. Y. R., Shin D. (2014) **Extensive conversion of hepatic biliary epithelial cells to hepatocytes after near total loss of hepatocytes in zebrafish** *Gastroenterology* **146** https://doi.org/10.1053/j.gastro.2013.10.019

[14] Goldshmit Y., Sztal T. E., Jusuf P. R., Hall T. E., Nguyen-Chi M., Currie P. D. (2012) **Fgf-dependent glial cell bridges facilitate spinal cord regeneration in zebrafish** *J. Neurosci* **32** https://doi.org/10.1523/JNEUROSCI.0758-12.2012

[15] Kroehne V., Freudenreich D., Hans S., Kaslin J., Brand M. (2011) **Regeneration of the adult zebrafish brain from neurogenic radial glia-type progenitors** *Development* **138** https://doi.org/10.1242/dev.072587

[16] Gemberling M., Bailey T. J., Hyde D. R., Poss K. D. (2013) **The zebrafish as a model for complex tissue regeneration** *Trends Genet* **29** https://doi.org/10.1016/j.tig.2013.07.003

[17] Papadimitriou C., et al. (2018) **3D Culture Method for Alzheimer's Disease Modeling Reveals Interleukin-4 Rescues Aβ42-Induced Loss of Human Neural Stem Cell Plasticity** *Dev. Cell* **46**:85–101 https://doi.org/10.1016/j.devcel.2018.06.005

[18] Mashkaryan V., et al. (2020) **Type 1 Interleukin-4 Signaling Obliterates Mouse Astroglia in vivo but Not in vitro** *Front. Cell Dev. Biol* **8**:1–16 https://doi.org/10.3389/fcell.2020.00114

[19] Ko S., Choi T., Russell J. O., So J., Shin D. (2016) **Bromodomain and extraterminal (BET) proteins regulate biliary-driven liver regeneration** *J. Hepatol* **64** https://doi.org/10.1016/j.jhep.2015.10.017.Bromodomain

[20] Goldshmit Y., et al. (2015) **Decreased anti-regenerative effects after spinal cord injury in spry4-/-mice** *Neuroscience* **287** https://doi.org/10.1016/j.neuroscience.2014.12.020

[21] Fausett B. V., Gumerson J. D., Goldman D. (2008) **The proneural basic helix-loop-helix gene Ascl1a is required for retina regeneration** *J. Neurosci* **28** https://doi.org/10.1523/JNEUROSCI.4853-07.2008

[22] Massoz L., Dupont M. A., Manfroid I. (2021) **Zebra-fishing for regenerative awakening in mammals** *Biomedicines* **9** https://doi.org/10.3390/biomedicines9010065

[23] Pisharath H. (2007) **Validation of nitroreductase, a prodrug-activating enzyme, mediated cell death in embryonic zebrafish (Danio rerio)** *Comp. Med* **57**:241–246

[24] Curado S., Anderson R. M., Jungblut B., Mumm J., Schroeter E., Stainier D. Y. R. (1970) **Conditional targeted cell ablation in zebrafish: A new tool for regeneration studies** *Dev. Dyn* **236**

[25] Pisharath H., Rhee J. M., a Swanson M., Leach S. D., Parsons M. J. (2007) **Targeted ablation of beta cells in the embryonic zebrafish pancreas using E.coli nitroreductase** *Mech Dev* https://doi.org/10.1016/j.mod.2006.11.005.Targeted

[26] Delaspre F., et al. (1970) **Centroacinar cells are progenitors that contribute to endocrine pancreas regeneration** *Diabetes* **64**

[27] Ghaye A. P., et al. (2015) **Progenitor potential of nkx6.1-expressing cells throughout zebrafish life and during beta cell regeneration** *BMC Biol* **13** https://doi.org/10.1186/s12915-015-0179-4

[28] Andersson O., et al. (2012) **Adenosine signaling promotes regeneration of pancreatic β-cells in vivo** *Cell Metab* https://doi.org/10.1016/j.cmet.2012.04.018.Adenosine

[29] Ye L., Robertson M. A., Hesselson D., Stainier D. Y. R., Anderson R. M. (2015) **Glucagon is essential for alpha cell transdifferentiation and beta cell neogenesis** *Dev* **142** https://doi.org/10.1242/dev.117911

[30] Helker C. S. M., et al. (2019) **A whole organism small molecule screen identifies novel regulators of pancreatic endocrine development** *Dev* **146** https://doi.org/10.1242/dev.172569

[31] Carril Pardo C., et al. (2022) **A delta-cell subpopulation with a pro-beta-cell identity contributes to efficient age-independent recovery in a zebrafish model of diabetes** *Elife*

[32] Singh S. P., et al. (2022) **A single-cell atlas of de novo β-cell regeneration reveals the contribution of hybrid β/δ-cells to diabetes recovery in zebrafish** *Development* **149** https://doi.org/10.1242/dev.199853

[33] Ninov N., Hesselson D., Gut P., Zhou A., Fidelin K., Stainier D. Y. R. (2013) **Metabolic regulation of cellular plasticity in the pancreas** *Curr. Biol* **23** https://doi.org/10.1016/j.cub.2013.05.037

[34] Parsons M. J., et al. (2009) **Notch-responsive cells initiate the secondary transition in larval zebrafish pancreas** *Mech. Dev* **126** https://doi.org/10.1016/j.mod.2009.07.002

[35] Ninov N., Borius M., Stainier D. Y. R. (2012) **Different levels of Notch signaling regulate quiescence, renewal and differentiation in pancreatic endocrine progenitors** *Development* **139** https://doi.org/10.1242/dev.076000

[36] Tornini V. A., et al. (2016) **Live Monitoring of Blastemal Cell Contributions During Appendage Regeneration** *Curr. Biol* https://doi.org/10.1016/j.cub.2016.08.072.Live

[37] McMillan S. C., et al. (2018) **A regulatory pathway involving retinoic acid and calcineurin demarcates and maintains joint cells and osteoblasts in regenerating fin** *Dev* **145** https://doi.org/10.1242/DEV.161158

[38] Cao Z., et al. (2021) **Calcineurin controls proximodistal blastema polarity in zebrafish fin regeneration** *Proc. Natl. Acad. Sci. U. S. A* **118** https://doi.org/10.1073/pnas.2009539118

[39] Kujawski S., et al. (2014) **Calcineurin Regulates Coordinated Outgrowth of Zebrafish Regenerating Fins** *Dev. Cell* **28** https://doi.org/10.1016/j.devcel.2014.01.019

[40] Tarifeño-Saldivia E., et al. (2017) **Transcriptome analysis of pancreatic cells across distant species highlights novel important regulator genes** *BMC Biol* **15** https://doi.org/10.1186/s12915-017-0362-x

[41] Heit J. J., et al. (2006) **Calcineurin/NFAT signalling regulates pancreatic β-cell growth and function** *Nature* **443** https://doi.org/10.1038/nature05097

[42] Lu J., et al. (2016) **IGFBP 1 increases β-cell regeneration by promoting α-to β-cell transdifferentiation** *EMBO J* **35** https://doi.org/10.15252/embj.201592903

[43] Karampelias C., et al. (2021) **Reinforcing one-carbon metabolism via folic acid/Folr1 promotes β-cell differentiation** *Nat. Commun* **12** https://doi.org/10.1038/s41467-021-23673-0

[44] Liu K. C., et al. (2017) **Inhibition of Cdk5 promotes β-cell differentiation from ductal progenitors** *Diabetes* **67** https://doi.org/10.2337/db16-1587

[45] Wu X., et al. (2010) **Calcineurin and ATF3: opposite roles in squamous skin cancer** *Nature* https://doi.org/10.1038/nature08996.Calcineurin

[46] Mammucari C., et al. (2005) **Integration of notch 1 and calcineurin/NFAT signaling pathways in keratinocyte growth and differentiation control** *Dev. Cell* **8** https://doi.org/10.1016/j.devcel.2005.02.016

[47] Kim Y. H., Larsen H. L., Rué P., Lemaire L. A., Ferrer J., Grapin-Botton A. (2015) **Cell Cycle–Dependent Differentiation Dynamics Balances Growth and Endocrine Differentiation in the Pancreas** *PLoS Biol* **13** https://doi.org/10.1371/journal.pbio.1002111

[48] Krentz N. A. J., et al. (2017) **Phosphorylation of NEUROG3 Links Endocrine Differentiation to the Cell Cycle in Pancreatic Article Phosphorylation of NEUROG3 Links Endocrine Differentiation to the Cell Cycle in Pancreatic Progenitors** *Dev. Cell* **41**:129–142 https://doi.org/10.1016/j.devcel.2017.02.006

[49] Flasse L. C., Stern D. G., Pirson J. L., Manfroid I., Peers B., Voz M. L. (2013) **The bHLH transcription factor Ascl1a is essential for the specification of the intestinal secretory cells and mediates Notch signaling in the zebrafish intestine** *Dev. Biol* **376** https://doi.org/10.1016/j.ydbio.2013.01.011

[50] Huttner W. B., Kosodo Y. (2005) **Symmetric versus asymmetric cell division during neurogenesis in the developing vertebrate central nervous system** *Curr. Opin. Cell Biol* **17** https://doi.org/10.1016/j.ceb.2005.10.005

[51] Ho A. D., Wagner W. (2007) **The beauty of asymmetry: Asymmetric divisions and self-renewal in the haematopoietic system** *Curr. Opin. Hematol* **14** https://doi.org/10.1097/MOH.0b013e3281900f12

[52] Bultje R. S., Castaneda-Castellanos D. R., Jan L. Y., Jan Y. N., Kriegstein A. R., Shi S. H. (2009) **Mammalian Par3 Regulates Progenitor Cell Asymmetric Division via Notch Signaling in the Developing Neocortex** *Neuron* **63** https://doi.org/10.1016/j.neuron.2009.07.004

[53] Guo M., Jan L. Y., Jan Y. N. (1996) **Control of daughter cell fates during asymmetric division: Interaction of Numb and Notch** *Neuron* **17** https://doi.org/10.1016/S0896-6273(00)80278-0

54. Sousounis K., et al. (2020) **K. Sousounis, et al., "Eya2 promotes cell cycle progression by regulating DNA damage response during vertebrate limb regeneration," 2020.** *Eya2 promotes cell cycle progression by regulating DNA damage response during vertebrate limb regeneration*

[55] Da S., et al. (2019) **S. Da et al., "Cell senescence contributes to tissue regeneration in zebrafish," no. July 2019, pp. 1–5, 2020, doi: 10.1111/acel.13052.** *Cell senescence contributes to tissue regeneration in zebrafish* :1–5 https://doi.org/10.1111/acel.13052

[56] Md Moin A. S., Butler P. C., Butler A. E. (2017) **Increased proliferation of the pancreatic duct gland compartment in type 1 diabetes** *J. Clin. Endocrinol. Metab* **102** https://doi.org/10.1210/jc.2016-3001

[57] Ghaye A. P., et al. (2015) **Progenitor potential of nkx6.1-expressing cells throughout zebrafish life and during beta cell regeneration** *BMC Biol* **13** https://doi.org/10.1186/s12915-015-0179-4

[58] Bergemann D., et al. (2018) **Nifurpirinol: A more potent and reliable substrate compared to metronidazole for nitroreductase-mediated cell ablations** *Wound Repair Regen* **26** https://doi.org/10.1111/wrr.12633

[59] Kwan K. M., et al. (2007) **The Tol2kit: a multisite gateway-based construction kit for Tol2 transposon transgenesis constructs** *Dev. Dyn. an Off. Publ. Am. Assoc. Anat* **236**:3088–3099 https://doi.org/10.1002/dvdy.21343

[60] Kawakami K. (2007) **Tol2: a versatile gene transfer vector in vertebrates** *Genome Biol* **8** https://doi.org/10.1186/gb-2007-8-s1-s7

Author information

Laura Massoz
Zebrafish Development and Disease Models laboratory, GIGA-Stem Cells, University of Liège, Liège, Belgium
For correspondence: laura.massoz@doct.uliege.be
ORCID iD: 0000-0002-4791-0920

David Bergemann
Zebrafish Development and Disease Models laboratory, GIGA-Stem Cells, University of Liège, Liège, Belgium

Arnaud Lavergne
Zebrafish Development and Disease Models laboratory, GIGA-Stem Cells, University of Liège, Liège, Belgium, GIGA-Genomics core facility, GIGA, University of Liège, Liège, Belgium

Célia Reynders
Zebrafish Development and Disease Models laboratory, GIGA-Stem Cells, University of Liège, Liège, Belgium

Caroline Désiront
Zebrafish Development and Disease Models laboratory, GIGA-Stem Cells, University of Liège, Liège, Belgium

Chiara Goossens
Zebrafish Development and Disease Models laboratory, GIGA-Stem Cells, University of Liège, Liège, Belgium

Lydie Flasse
Zebrafish Development and Disease Models laboratory, GIGA-Stem Cells, University of Liège, Liège, Belgium

Bernard Peers
Zebrafish Development and Disease Models laboratory, GIGA-Stem Cells, University of Liège, Liège, Belgium

Marianne L. Voz
Zebrafish Development and Disease Models laboratory, GIGA-Stem Cells, University of Liège, Liège, Belgium

Isabelle Manfroid
Zebrafish Development and Disease Models laboratory, GIGA-Stem Cells, University of Liège, Liège, Belgium

Editors

Reviewer #1 (Public Review):

Induction of beta cell regeneration is a promising approach for the treatment of diabetes. In this study, Massoz et.al., identified calcineurin (CaN) as a new potential modulator of beta cell regeneration by using zebrafish as model. They also showed that calcineurin (CaN) works together with Notch signaling calcineurin (CaN) to promote the beta cell regeneration. Overall, the paper is well organized, and technically sound. However, some evidence seems weak to get the conclusion.

Reviewer #2 (Public Review):

This work started with transcriptomic profiling of ductal cells to identify the upregulation of calcineurin in the zebrafish after beta-cell ablation. By suppressing calcineurin with its chemical inhibitor cyclosporin A and expressing a constitutively active form of calcineurin ubiquitously or specifically in ductal cells, the authors found that inhibited calcineurin activity promoted beta-cell regeneration transiently while ectopic calcineurin activity hindered beta-cell regeneration in the pancreatic tail. They also showed similar effects in the basal state but only when it was within a particular permissive window of Notch activity. To further investigate the roles of calcineurin in the ductal cells, the authors demonstrated that calcineurin inhibition additionally induced the proliferation of the ductal cells in the regenerative context or under a limited level of Notch activity. Interestingly, the enhanced proliferation was followed by a depletion of ductal cells, suggesting that calcineurin inhibition would exhaust the ductal cells. Based on the data, the authors proposed a very attractive and intriguing model of the role of calcineurin in maintaining the balance of the progenitor proliferation and the endocrine differentiation. However, the conclusions of this paper are only partially supported by the data as some evidence from the data remains suggestive.

1. In the transcriptomic profiling, genes differentially regulated in the ablated adults could be solely due to the chemical effects of metronidazole instead of the beta-cell ablation. A control group without ins:NTR-mCherry but treated with metronidazole is necessary to exclude the side effects of metronidazole.

2. Although it has been shown that the pancreatic duct is a major source of the secondary islets in the pancreatic tail in previous studies, there is no direct evidence showing the cyclosporin A-induced cells share the source in this manuscript. Without any proper lineage tracing work, the origin of those cyclosporin A-induced cells cannot be concluded.

3. It is interesting to see an increase of beta cells in the primary islet after cyclosporin A treatment (Supplemental Fig 2B). However, it remains unclear if their formation shares the same mechanism with the newly formed beta cells in the pancreatic tail.

4. The conclusion of the effect of cyclosporin A on the endocrine progenitors (Line 175) is not convincing because the data cannot distinguish the endocrine progenitors from the insulin-expressing cells. Indeed, Figure 2E shows that neurod1+ cells are fewer than ins+ cells (Figure 2D) in the pancreatic tail at 10 dpt, suggesting that all or at least the majority of neurod1+ cells are already ins+.

5. Figure 5D shows a significant loss of nkx6.1+ cells in the combined treatment group but there is no direct evidence showing this was a result of differentiation as the authors suggested. This cell loss also outnumbered the increase in ins+ cells (Figure 4D). The cell fates of these lost cells are still undetermined, and the authors did not demonstrate if apoptosis could be a reason of the cell loss.